RESEARCH OUTPUTS / RÉSULTATS DE RECHERCHE

Susceptibility of neuroblastoma and glioblastoma cell lines to SARS-CoV-2 infection

Bielarz, Valery; WILLEMART, KEVIN; Avalosse, Noémie; De Swert, Kathleen; Lotfi, Riselane; Lejeune, Noemie; Poulain, Florian; Ninanne, Noelle; Gilloteaux, Jacques; GILLET, NICOLAS; Nicaise, Charles

Link to publication

Citation for pulished version (HARVARD):
Bielarz, V, WILLEMART, KEVIN, Avalosse, N, De Swert, K, Lotfi, R, Lejeune, N, Poulain, F, Ninanne, N, Gilloteaux, J, GILLET, NICOLAS & Nicaise, C 2021, 'Susceptibility of neuroblastoma and glioblastoma cell lines to SARS-CoV-2 infection', *Brain research*, vol. 1758, 147344. https://doi.org/10.1016/j.brainres.2021.147344

Brain Research

Susceptibility of neuroblastoma and glioblastoma cell lines to SARS-CoV-2 infection
--Manuscript Draft--

Manuscript Number:	BRAINRES-D-20-01619R1
Article Type:	Research paper
Section/Category:	Neurobiology of Disease
Keywords:	sars-cov-2; Neuroblastoma; glioblastoma; neurotropism; cytopathic effect; susceptibility
Corresponding Author:	Charles Nicaise, Ph.D. Université de Namur BELGIUM
First Author:	Valéry Bielarz
Order of Authors:	Valéry Bielarz
	Kévin Willemart
	Noémie Avalosse
	Kathleen De Swert
	Riselane Lotfi
	Noémie Lejeune
	Florian Poulain
	Noelle Ninanne
	Jacques Gilloteaux
	Nicolas Gillet
	Charles Nicaise, Ph.D.
Manuscript Region of Origin:	BELGIUM
Abstract:	Modelling cell infection in-a-dish can represent a useful tool to understand the susceptibility of different cell types towards severe acute respiratory coronavirus-2 (SARS-CoV-2) and to decipher its neurotropism. In this perspective, retinoic acid (RA)-differentiated neuroblastoma cell lines, SH-SY5Y and SK-N-BE(2) and glioblastoma cell lines, U-87 MG and U-373 MG, were infected with a SARS-CoV-2 strain, at various multiplicity-of-infection (MOI). We first demonstrated that the common entry genes - needed for invading epithelial cells - were expressed. RA-differentiation induced an upregulation of ace2 and tmprss2 gene expression while inducing downregulation of ctsb and ctsl . Using in situ hybridization and confocal analysis, SARS-CoV-2 gene S RNA was detected intracellularly at MOI 5.0, and localized in both soma and neuritic-like or glial-like processes. The infection was confirmed by quantification of viral gene E RNA and showed a dose-dependency, with few infected cells at MOI 0.1. After 24 hours of infection, no cytopathic effect was observed in SH-SY5Y abilities to maintain neuritic processes or in U-373 MG for the uptake of glutamate. Unlike the permissive Vero E6 cells, no significant apoptosis death was detected following SARS-CoV-2 infection of neuroblastoma or glioblastoma cells. This study demonstrates the susceptibility of neuronal- and glial-like cell lines towards SARS-CoV-2 infection at high MOIs. Once inside the cells, the virus does not seem to rapidly replicate nor exert major cytopathic effect. Overall, our results strengthen the idea that SARS-CoV-2 has a tropism for nervous cells that express commonly described entry genes.

UNIVERSITÉ DE NAMUR

NARILIS
Namur Research Institute for Life Sciences

To :

**Brain Research
Editor-in-Chief**

Dr. Matthew J. LaVoie
University of Florida,
Gainesville, Florida, United States

Re: Manuscript Submission – *Brain Research*

December 10th, 2020

Dear Dr. Matthew J. LaVoie,

Enclosed for review at *Brain Research* is the manuscript entitled "Susceptibility of neuroblastoma and glioblastoma cell lines to SARS-CoV-2 infection". We believe that it will perfectly fit the scope of the section "Neurobiology of Disease".

In the context of the COVID-19 pandemic, we deciphered the susceptibility and permissiveness of neuroblastoma and glioblastoma cell lines towards SARS-CoV-2 infection. Knowing that the neurotropism of SARS-CoV-2 is more and more established, modelling cell infection in-a-dish can represent a useful tool to understand the CNS entry mechanisms and to develop therapeutic interventions that interfere with viral entry. Our main findings are that SARS-CoV-2 is able to invade neuroblastoma and glioblastoma cell lines, without exerting major cytopathic effect on either neuron-like morphology or on functional glutamate uptake. More interestingly, in all infected cells, the intracellular distribution included both the soma compartment and the neuritic-like or glial-like processes.

Below, you will find a list of potential experts/referees who recently published in the field of SARS-CoV-2 neurotropism.

I look forward to the comments of the reviewers. If there are any questions that I can answer, please feel free to contact me.

Sincerely yours,

Prof. Charles NICAISE
Université de Namur
Faculté de Médecine
URPhyM - NARILIS
Rue de Bruxelles, 61
B-5000 Namur, BELGIUM
Tél : +32 (0)81 72 42 56
Email : charles.nicaise@unamur.be

List of referees:

Dr. Lena SMIRNOVA
Johns Hopkins Bloomberg School of Public Health Department of Environmental Health & Engineering Center for Alternatives to Animal Testing (CAAT)
615 N Wolfe St, W7032
Baltimore, MD, 21205, USA
Email : lena.smirnova@jhu.edu

Dr. Jay GOPALAKRISHNAN
Institute of Human Genetics
University Hospital Düsseldorf
Heinrich-Heine-Universität, Düsseldorf, Germany
E-mail: jay.gopalakrishnan@hhu.de

Prof. Kwok-Yung YUEN
Department of Clinical Microbiology and Infection Control,
The University of Hong Kong-Shenzhen Hospital,
Shenzhen 518009, China
Email : kyyuen@hku.hk

Dr . Jian-Dong HUANG
Department of Microbiology,
Li Ka Shing Faculty of Medicine,
The University of Hong Kong
Pokfulam, Hong Kong, China
Email : jdhuang@hku.hk

To :

Brain Research
Editor-in-Chief
Dr. Matthew J. LaVoie
University of Florida,
Gainesville, Florida, United States

Brain Research
Senior Editor
Dr. Cesar V. Borlongan

Re: Manuscript Revision – *Brain Research* BRAINRES-D-20-01619

January 25th, 2021

Dear Dr. Matthew J. LaVoie,
Dear Dr. Cesar V. Borlongan,

Enclosed for publication at *Brain Research* is the revision of the manuscript entitled "Susceptibility of neuroblastoma and glioblastoma cell lines to SARS-CoV-2 infection".

We have addressed all of the comments of both reviewers. We have enclosed along with the manuscript a point-by-point set of responses to each reviewer comment, and we have made all of the necessary changes to the manuscript text. We appreciate the helpful comments of both reviewers, and we feel that the changes made based on their input have made for an improved manuscript.

I hope that you will be able to send this resubmission back to the original reviewers. If so, I look forward to their comments. If there are any questions that I can answer, please feel free to contact me.

Sincerely,

Dr. C. Nicaise
Université de Namur
Faculté de Médecine, URPhyM - NARILIS
Rue de Bruxelles, 61 – B-5000 NAMUR, Belgium
charles.nicaise@unamur.be

Reviewer Comments
Reviewer #1: In the present investigation, Bielarz and colleagues analyzed the neurotropism of SARS-COV-2. They used differentiated neuroblastoma cell lines and glioblastoma cell lines, at various multiplicity-of-infection (MOI). This study demonstrates the susceptibility of neuronal- and glial-like cell lines towards SARS-CoV-2 infection at high MOIs. Once inside the cells, the virus does not seem to rapidly replicate nor exert major cytopathic effect. Overall, these results confirmed that SARS-COV-2 has a strong neurotropism for nervous cells expressing ace2 and tmprss2. This investigation is of high interest for the scientific community and the experimental design as well the methods are adequate. However, this reviewer has some points to raise:
1)   The Authors should strengthen the Introduction section, reporting more references regarding SARS-COV-2 and the neurotropism.
Besides 16 references already listed in the introduction, we have included 5 most recent published findings about neuroinvasion abilities (Patterson et al.; Meinhardt et al.; Kumari et al.; Song et al.; Cantuti-Castelvetri et al.). Many other pending manuscripts can be found as preprints on free platforms (such as bioRxiv, medRxiv) and, from my point-of-view, I do not feel comfortable to refer those yet unpublished or (maybe) non-peer reviewed papers.

2)   Since the Authors analyzed also tmprss2, they should at least mention it in the introduction.
We have now added few sentences mentioning TMPRSS2 role in SARS-CoV-2 fusion activation as well as the distribution of entry proteins along the respiratory tract (page 5, line 24).

3)   The Authors should add the scale bar in Figure 1c.
We inserted a scale bar in Figure 2c (renumbered according to ref#2 suggestion).

Reviewer #2: The present study examined the susceptibility of neuroblastoma and glioblastoma cell lines to SARS-CoV-2 infection. These are interesting data. However, there are a few oversights that require the authors' attention.
1. In methods part, the authors need to briefly discuss the effect of cell culture media for U87 and U373 cell line.
Both cell lines are usually cultured in minimum essential growth medium (MEM) supplemented with 10% FBS. Lowering the serum concentration to 2% or to no-serum condition will definitely impact the cell behavior such as proliferation, adhesion, migration, secretome or abilities to form neurospheres (Motaln et al., Oncotarget, 2015). As we did not use serum-free medium in our experimental paradigm, we did not expect to induce major starvation stress. Although we did not assay it, we definitely observed a slower growth rate upon switching medium from 10% to 2%. We do not feel that the effect of medium or serum is worth discussing in the context of glioblastoma infection by SARS-CoV-2.

2. In cell culture media for SH-Sy5Y and SK-N-BE(2), why did the authors use low-serum medium?
While basal growth medium contains 10% FBS, the content of FBS is usually lowered to 2% FBS in the medium used for viral infection. This is a standard procedure, even that in some cases, the medium after infection is switched to a serum-free medium. We did not find any rational explanation in the scientific literature, and we postulate that serum-borne components (antibodies, thrombin,

plasminogen, complement factors …) interfere with viral adsorption by cleaving surface cell/virus entry receptors or inhibiting their interactions. According to ATCC recommendations, a low-serum condition is a standard procedure upon viral infection of cells in culture (https://www.atcc.org/~/media/PDFs/webinars/Presentations/2017/Culturing%20Viruses%20Webinar_10-2017.ashx). With respect to *in vitro* SARS-CoV-2 infection of nervous cells, only one publication mentioned the use of a serum-free medium during infection (Bullen et al., ALTEX, 2020), the others lacked this type of information.

3. The authors used RNAscope kit. Authors need to mention the RNAscope procedure in the methods section.
The procedure was already mentioned in the material and methods (see section 4.4.).

4. For figure 1, (a) the authors need to show counterstaining with nuclear marker, like Hoechst. (c) Also, the authors need to add scale bars in pictures.
Fluorescent *ish* pictures labeled with nCoV2019 probe are now counterstained with Hoechst in Figure 2a (renumbered according to ref's suggestion).

5. The authors need to rearrange the order of the figures with supplemental figures to match with the order as presented in the results section (ex fig1 -4).
We inserted the supplementary figure 1 as the figure 1 and renumbered the others accordingly.

1

Susceptibility of neuroblastoma and glioblastoma cell lines

to SARS-CoV-2 infection

4

5   Valéry Bielarz[1], Kévin Willemart[2], Noémie Avalosse[1], Kathleen De Swert[1], Riselane Lotfi[1],

6   Noémie Lejeune[2], Florian Poulain[2], Noelle Ninanne[3], Jacques Gilloteaux[1,4], Nicolas Gillet[2],

7   Charles Nicaise[1]

8

9   [1] URPhyM, NARILIS, Université de Namur, Namur, Belgium
10
11 [2] URVI, Université de Namur, Namur, Belgium
12
13 [3] URBC, Université de Namur, Namur, Belgium
14
15 [4] Department of Anatomical Sciences, St George's University School of Medicine, Newcastle upon Tyne,
16 United Kingdom
17
18
19 valery.bielarz@unamur.be; kevin.willemart@unamur.be;
20 noemie.avalosse@student.unamur.be; kathleen.deswert@unamur.be;
21 riselane.lotfi@student.unamur.be; noemie.lejeune@unamur.be; poulainflorian@gmail.com;
22 noelle.ninanne@unamur.be; JGilloteaux@sgu.edu; nicolas.gillet@unamur.be;
23 charles.nicaise@unamur.be
24
25

26 Correspondence to: Prof. Charles NICAISE

27 e-mail : charles.nicaise@unamur.be

28 Address: Université de Namur, URPhyM – NARILIS, Rue de Bruxelles 61, B-5000 Namur,

29 BELGIUM

30 Phone: +3281724256

31

32 **Abstract (< 250 words)**

1   Modelling cell infection in-a-dish can represent a useful tool to understand the susceptibility of

2   different cell types towards severe acute respiratory coronavirus-2 (SARS-CoV-2) and to

3   decipher its neurotropism. In this perspective, retinoic acid (RA)-differentiated neuroblastoma

4   cell lines, SH-SY5Y and SK-N-BE(2) and glioblastoma cell lines, U-87 MG and U-373 MG,

5   were infected with a SARS-CoV-2 strain, at various multiplicity-of-infection (MOI). We first

6   demonstrated that the common entry genes - needed for invading epithelial cells - were

7   expressed. RA-differentiation induced an upregulation of *ace2* and *tmprss2* gene expression

8   while inducing downregulation of *ctsb* and *ctsl*. Using *in situ* hybridization and confocal

9   analysis, SARS-CoV-2 *gene S* RNA was detected intracellularly at MOI 5.0, and localized in

10   both soma and neuritic-like or glial-like processes. The infection was confirmed by

11   quantification of viral *gene E* RNA and showed a dose-dependency, with few infected cells at

12   MOI 0.1. After 24 hours of infection, no cytopathic effect was observed in SH-SY5Y abilities

13   to maintain neuritic processes or in U-373 MG for the uptake of glutamate. Unlike the

14   permissive Vero E6 cells, no significant apoptosis death was detected following SARS-CoV-2

15   infection of neuroblastoma or glioblastoma cells. This study demonstrates the susceptibility of

16   neuronal- and glial-like cell lines towards SARS-CoV-2 infection at high MOIs. Once inside

17   the cells, the virus does not seem to rapidly replicate nor exert major cytopathic effect. Overall,

18   our results strengthen the idea that SARS-CoV-2 has a tropism for nervous cells that express

19   commonly described entry genes.

1   **Keyword**s

2   SARS-CoV-2, neuroblastoma, glioblastoma, neurotropism, cytopathic effect, susceptibility

3

4

5   **Abbreviations**

6   SARS-CoV   severe acute respiratory syndrome coronavirus

7   SARS-CoV-2   severe acute respiratory syndrome coronavirus-2

8   COVID-19   coronavirus disease 2019

9   ace2   angiotensin-converting enzyme 2

10 tmprss2   transmembrane protease, serine 2

11 ctsb   cathepsin B

12 ctsl   cathepsin L

13 MOI   multiplicity-of-infection

14 ish   *in situ* hybridization

15 hprt   hypoxanthine-guanine phosphoribosyltransferase

16 RA   retinoic acid

17 BBB   blood-brain barrier

18

19

20 **Highlights**

21 * Neuroblastoma and glioblastoma cells express SARS-CoV-2 entry genes

22 * Neuroblastoma and glioblastoma cell lines are susceptible to SARS-CoV-2 infection

23 * Viral RNA is detected intracellularly in both soma and cell's extensions

24 * SARS-CoV-2 does not exert cytopathic effect on neuroblastoma or glioblastoma cells

25

Bielarz *et al.*   SARS-CoV-2 infection of neural cell lines

Highlights

* Neuroblastoma and glioblastoma cells express SARS-CoV-2 entry genes

* Neuroblastoma and glioblastoma cell lines are susceptible to SARS-CoV-2 infection

* Viral RNA is detected intracellularly in both soma and cell's extensions

* SARS-CoV-2 does not exert cytopathic effect on neuroblastoma or glioblastoma cells

Susceptibility of neuroblastoma and glioblastoma cell lines to SARS-CoV-2 infection

Valéry Bielarz[1], Kévin Willemart[2], Noémie Avalosse[1], Kathleen De Swert[1], Riselane Lotfi[1],

Noémie Lejeune[2], Florian Poulain[2], Noelle Ninanne[3], Jacques Gilloteaux[1,4], Nicolas Gillet[2],

Charles Nicaise[1]

[1] URPhyM, NARILIS, Université de Namur, Namur, Belgium

[2] URVI, Université de Namur, Namur, Belgium

[3] URBC, Université de Namur, Namur, Belgium

[4] Department of Anatomical Sciences, St George's University School of Medicine, Newcastle upon Tyne, United Kingdom

valery.bielarz@unamur.be; kevin.willemart@unamur.be; noemie.avalosse@student.unamur.be; kathleen.deswert@unamur.be; riselane.lotfi@student.unamur.be; noemie.lejeune@unamur.be; poulainflorian@gmail.com; noelle.ninanne@unamur.be; JGilloteaux@sgu.edu; nicolas.gillet@unamur.be; charles.nicaise@unamur.be

Correspondence to: Prof. Charles NICAISE

e-mail : charles.nicaise@unamur.be

Address: Université de Namur, URPhyM – NARILIS, Rue de Bruxelles 61, B-5000 Namur, BELGIUM

Phone: +3281724256

Abstract (< 250 words)

Modelling cell infection in-a-dish can represent a useful tool to understand the susceptibility of different cell types towards severe acute respiratory coronavirus-2 (SARS-CoV-2) and to decipher its neurotropism. In this perspective, retinoic acid (RA)-differentiated neuroblastoma cell lines, SH-SY5Y and SK-N-BE(2) and glioblastoma cell lines, U-87 MG and U-373 MG, were infected with a SARS-CoV-2 strain, at various multiplicity-of-infection (MOI). We first demonstrated that the common entry genes - needed for invading epithelial cells - were expressed. RA-differentiation induced an upregulation of *ace2* and *tmprss2* gene expression while inducing downregulation of *ctsb* and *ctsl*. Using *in situ* hybridization and confocal analysis, SARS-CoV-2 *gene S* RNA was detected intracellularly at MOI 5.0, and localized in both soma and neuritic-like or glial-like processes. The infection was confirmed by quantification of viral *gene E* RNA and showed a dose-dependency, with few infected cells at MOI 0.1. After 24 hours of infection, no cytopathic effect was observed in SH-SY5Y abilities to maintain neuritic processes or in U-373 MG for the uptake of glutamate. Unlike the permissive Vero E6 cells, no significant apoptosis death was detected following SARS-CoV-2 infection of neuroblastoma or glioblastoma cells. This study demonstrates the susceptibility of neuronal- and glial-like cell lines towards SARS-CoV-2 infection at high MOIs. Once inside the cells, the virus does not seem to rapidly replicate nor exert major cytopathic effect. Overall, our results strengthen the idea that SARS-CoV-2 has a tropism for nervous cells that express commonly described entry genes.

2

Keywords

SARS-CoV-2, neuroblastoma, glioblastoma, neurotropism, cytopathic effect, susceptibility

Abbreviations

SARS-CoV	severe acute respiratory syndrome coronavirus
SARS-CoV-2	severe acute respiratory syndrome coronavirus-2
COVID-19	coronavirus disease 2019
ace2	angiotensin-converting enzyme 2
tmprss2	transmembrane protease, serine 2
ctsb	cathepsin B
ctsl	cathepsin L
MOI	multiplicity-of-infection
ish	*in situ* hybridization
hprt	hypoxanthine-guanine phosphoribosyltransferase
RA	retinoic acid
BBB	blood-brain barrier

Highlights

* Neuroblastoma and glioblastoma cells express SARS-CoV-2 entry genes

* Neuroblastoma and glioblastoma cell lines are susceptible to SARS-CoV-2 infection

* Viral RNA is detected intracellularly in both soma and cell's extensions

* SARS-CoV-2 does not exert cytopathic effect on neuroblastoma or glioblastoma cells

3

1. Introduction

Most of the time, the infection with severe acute respiratory syndrome coronavirus 2 (SARS-CoV-2) causes respiratory symptoms, known as coronavirus disease 2019 (COVID-19), although a minority of patients are at risk of developing a severe form with extrapulmonary involvements (for review (Gupta et al., 2020)). Severely SARS-CoV-2-affected patients are more likely to develop neurologic symptoms (e.g. headache, epilepsy, confusion, nausea and vomiting) than patients with a mild form of COVID-19 (Asadi-Pooya and Simani, 2020; Mao et al., 2020a; Paterson et al., 2020). Among the worst neurologic cases, viral encephalitis, necrotizing encephalopathy, acute myelitis or Guillain-Barré syndrome were reported (Chen et al., 2020; Kilinc et al., 2020; Mao et al., 2020a; Moriguchi et al., 2020; Poyiadji et al., 2020; Zhao et al., 2020). Intriguingly, some patients developed neurologic symptoms even prior to any respiratory manifestation. In one retrospective study, up to 88% among the severe patients showed acute cerebrovascular diseases associated with impaired consciousness (Mao et al., 2020b). Neuro-imaging supports substantial brain damages in both COVID-19 survivors and non-survivors (Coolen et al., 2020; Helms et al., 2020; Zanin et al., 2020). Increasing evidences show the presence of SARS-Cov-2 in brain *post-mortem* tissue (Bulfamante et al., 2020; Paniz-Mondolfi et al., 2020; Puelles et al., 2020; Song et al., 2021), even though the mechanisms and routes of CNS entry are still elusive.

SARS-CoV-2 belongs to the same beta-coronaviruses family as SARS-CoV (2003 China outbreak) and shares up to 79,6% pairwise identities on a genomic level with its cousin (Lu et al., 2020). SARS-CoV-2 also shares common entry mechanisms used to invade target cells, including the binding of the spike (S) protein to human ACE2 receptor. S protein sequence was found to be approximately 77% homologous between SARS-CoV-2 and SARS-CoV. SARS-CoV-2 entry also depends on TMPRSS2 protease activity, which helps at ACE2 cleavage and receptor-binding domain unmasking, a condition required for membrane fusion (Hoffmann et

4

al., 2020). Alternatively, cathepsin B or L may be able to substitute for TMPRSS2 in early endosomes upon endocytosis. ACE2 and TMPRSS2 have been detected at high expression levels in nasal, bronchial epithelium, as well as in alveolar epithelium (mostly type II pneumocytes), which explains the central respiratory pathology (Ortiz et al., 2020). Previously, neuro-invasion abilities of SARS-CoV have been firmly demonstrated on both patients and experimental animal models (Gu et al., 2005; Netland et al., 2008). Evidence from transgenic humanized ACE2 mice showed that SARS-CoV is able to enter the nervous system through the neuro-olfactory epithelium. It is then carried along the olfactory nerve up to the olfactory bulb, where it starts to spread to neighboring nervous cells (Netland et al., 2008). Similar SARS-CoV-2 neurotropic properties and CNS entry routes are under investigation. Of note, infected cells from the olfactory neuro-epithelium are suggested as gateways to central nervous system invasion in some individuals with COVID-19 (Cantuti-Castelvetri et al., 2020; Meinhardt et al., 2020). Such an entry route was demonstrated as plausible in transgenic humanized ACE2 mice following experimental intranasal instillation of SARS-CoV-2 (Kumari et al., 2021).

So far, *in vitro* data showed the permissiveness of U-251 glioblastoma cell line to SARS-CoV-2 infection (Chu et al., 2020). Recently, evidences from ~~four~~ five independent groups converge to show that human neural progenitor cells, grown either as neurospheres or as brain organoids, are susceptible to SARS-CoV-2 infection (Bullen et al., 2020; Ramani et al., 2020; Song et al., 2021; Yang et al., 2020; Zhang et al., 2020). In the present report, we aim at investigating the susceptibility of neuroblastoma and glioblastoma cell lines towards SARS-CoV-2 infection. These respective neuron-like and glial-like cells might represent useful tools to decipher the entry, replication and cytopathic effect of SARS-CoV-2 in the CNS.

Formatted: Line spacing: Double

5

2. Results

Before infecting the various neural cell lines with a Belgian SARS-CoV-2 strain, we sought to explore their expression level of entry genes, encoding proteins commonly needed by SARS-CoV-2 for invading human host cells. The transcripts for *ace2* and *tmprss2* genes were detected in both neuroblastoma (SH-SY5Y and SK-N-BE(2)) and both glioblastoma (U-87 MG and U-373 MG) cells, however in lower amounts than those of *hprt* housekeeping gene (~~Suppl.~~ Fig~~ure~~ 1a). Interestingly, RA-driven neuronal differentiation in SH-SY5Y and SK-N-BE(2) induced a significant upregulation of *ace2* mRNA, compared to undifferentiated cells (0.0007197±7.698e-005 *vs.* 0.003234±0,0005701 in SH-SY5Y, p<0.05; 0.004433±0.00107 *vs.* 0.01072± 0.001291 in SK-N-BE(2), p<0.05). Similarly, *tmprss2* gene expression was significantly induced upon RA differentiation (0.0008177±6.422e-005 *vs.* 0.005994±0.0008207 in SH-SY5Y, p<0.05; 0.05964±0.02418 *vs.* 0.1956±0.008158 in SK-N-BE(2), p<0.05, RA-differentiated cells *vs.* undifferentiated cells). No comparison was made between cell lines due to variable amounts of *hprt* housekeeping gene. The transcripts of cathepsin B and L were expressed at higher levels than *hprt* across all cell lines analyzed (~~Suppl.~~ Fig~~.~~ ure 1b). RA-induced differentiation produced a significant downregulation of *ctsb* mRNA in SK-N-BE(2) cells (27.61±2.809 *vs.* 21.35±1.185, p=0.05). Additionally, RA-induced differentiation produced a significant downregulation of *ctsl* mRNA in both SH-SY5Y and SK-N-BE(2) (4.317±0.8435 *vs.* 2.311±0.1334, p<0.05; 10.99±1.412 *vs.* 4.942±0.4085, p<0.05, RA-differentiated cells *vs.* undifferentiated cells).

RA-differentiated SH-SY5Y and SK-N-BE(2) were infected with SARS-CoV-2 at various MOIs during 2 or 24 hours. Viral RNA was revealed using fluorescent or chromogenic *in situ* hybridization (*ish*) targeting the *gene S*. After 24 hours at a MOI 5.0 of infection, *ish* signal was visualized in the cell bodies (black arrow), and to a certain extent in the neuritic processes (arrowheads in Figure ~~1a~~2a). At MOI 0.1 and 1.0, *ish* signal was much sparser, probably

6

reflecting a fewer number of infected neuroblastoma cells (data not shown). In comparison, infection of highly permissive VeroE6 cells with a MOI of 0.1 during 24 hours produces a massive *ish* signal in the cytoplasmic compartment (Figure 1a2a). The entry of viral particles in neuroblastoma cell lines was quantified using a qRT-PCR targeting the SARS-CoV-2 *gene E* (Figure 1b2b). In SH-SY5Y, a 24 hours infection with MOIs 1.0 and 5.0 produced a significant amplification of SARS-CoV-2 RNA from lyzed cells, in a dose-dependent manner (respectively 1.398±0.0976, p<0.05; 10.73±0.7595, p<0.001 when compared to mock condition). Noteworthy, the relative amount of *gene E* detected was higher when SH-SY5Y cells were infected at MOI 5.0 for 24 hours than for 2 hours (10.73±0.7595 vs. 5.713±0.1542, p<0.001). In SK-N-BE(2) cells, only the highest MOI produced a significant infection at both timings, when compared to mock condition (respectively 1.443±0.4262, p<0.001 and 1.284±0.09506, p<0.001). No difference of viral RNA amount was observed between 2 hours and 24 hours of infection. Given that neither transmitted light microscopy or qRT-PCR assays could provide a definitive answer about the viral entry – i.e. viral particles could be adsorbed at the cell surface non-specifically or receptor-bound – into host cells, we assessed the intracellular localization of viral RNA by confocal analysis. The cytoskeleton of SH-SY5Y and SK-N-BE(2) cells was visualized using immunofluorescence against α-tubulin while SARS-CoV-2 gene S was revealed using fluorescent *ish* (Figure 1c2c). In both cell lines, viral RNA was found in the same confocal plane as α-tubulin network. Further analysis of fluorescence intensity confirmed that fluorescent peaks, corresponding to SARS-CoV-2 gene S (red) and to α-tubulin (green), were overlapping (asterix in Suppl. Fig. 21).

We next investigated a cytopathic effect of SARS-CoV-2 once inside the cells by measuring the length of neuritic processes grown by RA-differentiated SH-SY5Y (Figure 1d2d). No effect of SARS-CoV-2 infection was observed on the abilities of differentiated SH-SY5Y cells to maintain their neurites, even at the highest MOI of 5.0 after 24 hours of infection (52.72±2.167

1 μm compared to 52.98±2.037 μm in mock condition, p=n.s.). In the same line, we sought to

2 know whether SARS-CoV-2 could induce cell death in infected nervous cell lines. The

3 apoptosis rate was quantified in VeroE6 cells and compared to infected SH-SY5Y and SK-N-

4 BE(2) cells (Figure ~~1e~~2e). While VeroE6 cells are highly permissive to SARS-CoV-2 (Figure

5 ~~1a~~2a) and are therefore used to amplify the virus, many of infected cells undergo apoptosis-

6 mediated cell death upon replication and/or release of viral particles. In VeroE6, the number of

7 cleaved caspase-3 immunoreactive cells reached up to 25.33±2.603 % upon exposure to MOI

8 5.0 during 24 hours, compared to 2.000±0.5774 % in mock condition (p<0.001). Interestingly,

9 neither SH-SY5Y or SK-N-BE(2) showed overt apoptosis upon infection with SARS-CoV-2,

10 at any MOIs tested. For instance, the percentages of apoptotic cells were respectively 3.66±2.66

11 % and 7.00±4.04 % at MOI 5.0 in SH-SY5Y and SK-N-BE(2) (p=n.s., compared to 2.50±0.88

12 % in mock conditions). Overall, both neuroblastoma cell lines were much less prone to

13 apoptosis than VeroE6 cells at comparable MOIs (two-way ANOVA, VeroE6 *vs.* SH-SY5Y:

14 $F_{(1,16)}$=44.21, p<0.001; VeroE6 *vs.* SK-N-BE(2) : $F_{(1,16)}$=30.61, p<0.001).

15 In order to evaluate the susceptibility of neural cell lines closer to a glial phenotype, U-87 MG

16 and U-373 MG glioblastoma cell lines were infected with SARS-CoV-2 according to the same

17 paradigm as neuroblastoma cells. At 2- or 24-hours post-infection, viral RNA was revealed

18 using chromogenic *in situ* hybridization targeting the *gene S* (Figure ~~2a~~3a). Following 24 hours

19 at MOI 5.0, infected cells showed obvious *ish* chromogenic deposits in the cell bodies as well

20 as in the glial-like processes (inset in Figure 2a). The entry of viral particles in glioblastoma

21 cells was also quantified using qRT-PCR (Figure ~~3~~2b). In U-87 MG cells, a 24-hour infection

22 produced a significant amplification of SARS-CoV-2 RNA, in a dose-dependent manner

23 (0.323±0.05743 for MOI 1.0, p<0.01 and 1.125±0.07618 for MOI 5.0, p<0.001 compared to

24 mock condition). Even though the levels of infection followed a similar profile at 2 hours post-

25 infection, the relative amount of SARS-CoV-2 *gene E* was significantly lower at 24 hours than

1   at 2 hours of infection for MOI 5.0 (1.125±0.07618 vs. 1.617±0.1079, p<0.001). In U-373 MG,

2   only the highest MOI at 2 hours of infection led to a significant detection of viral RNA,

3   compared to mock condition (2.117±0.2568 *vs.* 0.0±0.0 undetected, p<0.001) (Figure 2b3b). A

4   24-hour infection produced a significant amplification in a dose-dependent manner

5   (0.9433±0.0382 for MOI 1.0, p<0.01 and 3.671±0.4731 for MOI 5.0, p<0.001 compared to

6   mock condition). At MOI 5.0, a longer infection time led to increased amount of *gene E*

7   detected in U-373 MG (2.117±0.2568 at 2 hours vs. 3.671±0.4731 at 24 hours, p<0.001).

8   U-87 and U-373 cell lines are both considered as glioblastoma cells comprising a heterogeneous

9   mixture of morphologically, biochemically and functionally distinct cancer cells. For instance,

10   they are both classified as astrocytoma cells but differ in terms of GFAP expression. Grown on

11   uncoated plastic culture dishes, U-87 MG cells are GFAP^{low} expressing cells whereas U-373

12   MG cells are GFAP^{high}-expressing cells (Figure 2c3c). Both cell lines, no matter they express

13   low or high GFAP levels, are susceptible to SARS-CoV-2 infection. U-87 and U-373 also differ

14   in glutamate uptake abilities, even though all glioma cell lines showed impaired glutamate

15   uptake compared to normal human astrocytes (Ye and Sontheimer, 1999). While U-87 cells

16   have lost this ability (data not shown), U-373 MG cells internalized glutamate upon addition of

17   200 µM of glutamate in the medium (111.4±3.452 µM compared to 224.7±8.722 µM in basal

18   medium without cells, p<0.001) (Figure 2d3d). Infection with various MOIs of SARS-CoV-2

19   during 24 hours did not impact U-373 cells in their glutamate uptake abilities (one-way

20   ANOVA, p= 0.4668 mock *vs.* MOI 0.1; p=0.0955 mock *vs.* MOI 1.0; p=0.9664 mock *vs.* MOI

21   5.0). Finally, SARS-CoV-2 cytopathic effect on glioblastoma cells was evaluated by counting

22   the number of cleaved caspase-3 positive cells at 24 hours of infection (Figure 2e3e). Infected

23   U-87 or U-373 did not show more apoptosis at any MOI tested than mock condition. For

24   instance, the percentages of apoptotic cells were respectively 5.00±3.60% and 8.33±0.88 % at

9

1   MOI 5.0 in U-87 and U-373 (p=n.s., compared to 2.83±0.83 % in mock conditions). Overall,

2   glioblastoma cell lines were much less prone to apoptotic cell death than VeroE6 cells at

3   comparable MOIs (two-way ANOVA, VeroE6 *vs.* U-87 MG: $F_{(1,16)}$=38.70, p<0.001; VeroE6

4   *vs.* U-373 MG : $F_{(1,16)}$=38.78, p<0.001).

5

6

7

10

3. Discussion

Our main findings are that SARS-CoV-2 is able to invade neuroblastoma and glioblastoma cell lines, without exerting major cytopathic effect on either neuron-like morphology or on functional glutamate uptake, and without inducing obvious apoptosis. Although the viral entry-dependency on common entry genes was not investigated, a basal expression of ace2, tmprss2, cathepsin B and cathepsin L transcripts was detected in all cell lines. Noteworthy, RA-differentiated neuroblastoma cells upregulated the gene expression of surface receptors such as ace2 and tmprss2. The definitive entry mechanisms inside nervous cells are still debated and existence of alternative surface receptors that might be hijacked cannot be ruled out, as it is described for SARS-CoV and some epithelial cells or immune cells e.g. CD147/BSG, CD26/DPP4 (Radzikowska et al., 2020).

Our experimental design allows to conclude that neuroblastoma and glioblastoma cells are modestly susceptible to SARS-CoV-2 infection, based on the high MOI needed to infect cells. In comparison to recent studies, human brain organoids and neurospheres were respectively infected with MOIs of 10.0 and 0.1 (Bullen et al., 2020; Zhang et al., 2020). At early infection timings (24h), neuroblastoma and glioblastoma cells were not as permissive as VeroE6 epithelial cells. So far, contradictory results are reported about the SARS-CoV-2 replication into human neurons. While one study showed that SARS-CoV-2 entered neurons from brain organoids but did not replicate (Ramani et al., 2020), in two studies genomic viral material was found in the supernatant at higher level several hours post-infection than at the time zero of infection, which supports the release of new viral particles (Bullen et al., 2020; Zhang et al., 2020). Intriguingly, we did not observe major SARS-CoV-2 cytopathic effect on any cell lines, unlike what was described in infected brain neurospheres or despite the evidences of neuronal and astrocytic injury in COVID-19 patients (Kanberg et al., 2020; Ramani et al., 2020). This

11

1   might be explained by a better resistance of tumor cell lines towards SARS-CoV-2 infection or

2   a too short timing for apoptosis analysis.

3   Bearing in mind the limitation that *in situ* hybridization – and not immunofluorescence nor

4   electron microscopy - was used throughout this study to detect SARS-CoV-2, our confocal

5   images comforted the intracellular localization of viral RNA. Interestingly, viral RNA was

6   distributed in both soma, and neuron-like or glial-like extensions. So far, we did not investigate

7   whether this distribution was due to random internalization along the cell membrane or whether

8   internalized viral particles were able to be transported inside/along the cell processes. This last

9   concept is relevant for deciphering the CNS entry routes. Among the entry pathways, the

10 retrograde transport along nerve fibers from peripheral infected tissues (i.e. nasal cavity) or the

11 hematogenous pathway across the blood-brain barrier (BBB) are being demonstrated

12 (Meinhardt et al., 2020; Uversky et al., 2020). From our images showing SARS-CoV-2 RNA

13 in the cell processes, it is tempting to hypothesize that neuron-like or glial-like cells might

14 internalize viral particles at their farthest cell extension and then, using intracellular trafficking,

15 carry them back to the soma. Corollary, SARS-CoV-2 might penetrate the CNS gate by first

16 invading brain endothelial cells or following BBB disruption, then being caught at the

17 perivascular astrocytic processes (Uversky et al., 2020). This hypothesis is supported by

18 ultrastructural findings from autopsied COVID-19 patients, where authors captured viral

19 particles at the endothelial-astrocyte interface (Bulfamante et al., 2020; Paniz-Mondolfi et al.,

20 2020). This passage would even be eased in the context of an important systemic inflammation

21 that includes cytokines known to compromise BBB integrity (Uversky et al., 2020).

22 This study on SARS-CoV-2 cell tropism is complementary to those using human pluripotent

23 stem cell-based platform (Yang et al., 2020). Infection of neuroblastoma or glioblastoma cells

24 might serve as an easy and low-cost model for testing drugs that interfere with viral entry, e.g.

25 ACE2 neutralizing antibodies, or other viral life cycle targets.

12

1 **4. Experimental Procedure**

2 **4.1. Cell culture**

3 The SH-SY5Y neuroblastoma cell line, U-87 MG and U-373 MG glioblastoma cell lines were

4 kindly provided by Profs. Jean-Pierre Brion and Karelle Leroy (Université Libre de Bruxelles,

5 BE). The SK-N-BE(2) neuroblastoma cell line was a kind gift from Prof. Marielle Boonen

6 (Université de Namur, BE). All cell lines were used between passage 15 and 25. They were

7 maintained in DMEM/F12 (Life Technologies, Grand Island, NY, USA) supplemented with 10

8 % fetal bovine serum (Sigma-Aldrich, Overijse, BE) and penicillin/streptomycin (Sigma-

9 Aldrich, Overijse, BE / Millipore, USA). Cells were grown in a sterile incubator at 37 °C, 95

10 % air humidity and 5 % CO_2 concentration. Culture medium was changed twice a week,

11 depending on cell density, and cells were passaged for further cultivation or differentiation

12 experiment at 80 – 90 % confluency. For passaging, cells were trypsinized using 0.05 %

13 Trypsin/EDTA during 2 minutes, washed in medium and spun down at 130 g for 7 minutes and

14 further split at a ratio 1:10. For differentiation experiment, SH-SY5Y and SK-N-BE(2) cells

15 were seeded at a density of 20,000 cells per cm2, on glass coverslips pre-coated with 0.1 mg/ml

16 Poly-L-lysine (Sigma-Aldrich, Overijse, BE). A differentiation protocol was applied based on

17 7 day-exposure to 10 µM all-trans-retinoic acid (RA) (Sigma-Aldrich, Overijse, BE) added in

18 low-serum medium (DMEM/F12 + 2% FBS + penicillin/streptomycin). RA-driven

19 differentiation was initiated 24 h after seeding and fresh medium was replaced everyday up to

20 day 7. Vero cells, clone E6 (VeroE6), were used to amplify a purified SARS-CoV-2 strain

21 isolated from a Belgian COVID-19 patient.

22 **4.2. Infection with SARS-CoV-2**

23 All infections or viral amplification were performed in a biosafety level-3 laboratory

24 (Université de Namur, BE). The SARS-CoV-2 isolate was kindly provided by Prof. Piet Maes

25 (KULeuven, BE). The viral titer of SARS-CoV-2 strain was determined by TCID50 on culture

13

supernatant from infected Vero E6 cells. Neuroblastoma or glioblastoma cells were plated at a

density of 20,000 cells per cm2 in a 24-well plate for *in situ* hybridization or a 12-well plate for

gene expression studies. Cells were infected during 2- or 24- hours using a multiplicity-of-

infection (MOI) of 0.1, 1.0 or 5.0 in low-serum medium. For mock condition, cells were

incubated with the low-serum medium-only. At the end of infection, culture medium was

carefully discarded. Cells were thoroughly washed three times with PBS and either lyzed in

TriZol or chemically-fixed with 4% paraformaldehyde, ensuring virus inactivation.

4.3. RNA isolation and qRT-PCR

Cells were homogenized in 1 mL of Trizol reagent and total RNA was further isolated according

to manufacturer's instructions (Life Technologies, Bleiswijk, NL). RNA concentrations were

measured using a spetrophotometer Nanodrop 1000 (Thermo Scientific, Bleiswijk, NL). Total

RNAs (1µg), including viral and human RNAs, were reverse-transcribed using the Super Script

II RNase H reverse transcriptase kit according to manufacturer's instructions (Invitrogen,

Merelbeke, BE). cDNA was used to amplify SARS-CoV-2 *gene E* with Takyon Taqman kit

and human genes with Takyon SYBR Green kit (Eurogentec, Liège, BE) in a Light Cycler 96

device (Roche Diagnostics, Mannheim, DE) (Coupeau et al., 2020). Primer sequences are listed

in Table 1. Relative gene expression was computed using the $\delta\Delta$Cq method with *hprt* as

housekeeping gene.

4.4. in situ hybridization and immunofluorescence

Coverslips were fixed in cold 4% paraformaldehyde during 15 20 minutes and then washed and

stored in PBS at 4°C. Fixed cells were used within one-week post-fixation. Expression of

SARS-CoV-2 *gene S* was detected according to manufacturer's kit instructions (RNAScope,

Advanced Cell Diagnostics, Bio-techne, Abingdon, UK) and by using a specific target probe

(RNAscope Probe-V-nCoV2019-S, #848561, Bio-techne, Abingdon, UK). Briefly, cells were

permeabilized with PBS plus 0.1% Tween 20 for 10 min. After washing, endogenous

14

1   peroxidases were blocked with hydrogen peroxide for 10 min followed by 2 washes in PBS.

2   Cells were then incubated with RNAScope® Protease III (Advanced Cell Diagnostics Inc,

3   Hayward, USA) for 10 min. and subsequently washed in PBS. Samples were incubated with

4   the probe specifically targeting SARS-CoV-2 *gene S* mRNA (RNAScope, #422511, Advanced

5   Cell Diagnostics, Bio-techne, Abingdon, UK) for 2 hours at 40°C and then washed for 2min in

6   RNAScope® wash buffer (Advanced Cell Diagnostics, Bio-techne, Abingdon, UK).

7   Amplification rounds 1-6 alternated from 30 to 15 min at 40°C. Between each amplification

8   round, samples were washed with RNAScope® wash buffer. Detection of probe signals was

9   performed by incubating samples with alkaline phosphatase (solution of RNAScope® Fast B

10   and A ratio 1:60) for 10 min. at room temperature. Samples were then washed in milliQ water.

11   Following *ish*, samples were either counterstained with hematoxylin (Sigma-Aldrich, Overijse,

12   BE), dried for 30 min. at 60°C and mounted using VectaMount® (Vector Laboratories,

13   Burlingame, USA) or fluorescently stained according to the protocol below.

14   For *ish*/immunofluorescence multiplexing, coverslips were further washed 5 min at RT in PBS.

15   Non-specific binding was blocked in a PBS-BSA 1% for 30min at RT. Then, samples were

16   incubated with primary antibodies in PBS-BSA 1 % buffer overnight at RT: α-tubulin (1:500,

17   T-5168, Sigma-Aldrich); GFAP (1:1000, G-3893, Sigma-Aldrich); cleaved caspase-3 (1:1000,

18   #9664, Cell Signaling). After that, samples were washed 3X5 min with PBS-BSA 1%.

19   Fluorophore-coupled secondary antibodies alexa fluor® 488 goat anti-mouse IgG 1:200

20   (#A11001, Life Technologies, Oregon, USA) or goat anti-rabbit IgG 1:200 (#A11008, Life

21   Technologies, Oregon, USA) in PBS-BSA1% were applied on their respective tissue sections

22   and incubated for 30 min at RT. Afterwards, they were washed 3X5 min with PBS-BSA 1%

23   and cell nuclei were stained in a solution of Hoechst 33258 (Life Technologies, Oregon, USA).

24   Finally, after 1X5 min wash with PBS-BSA 1% and 2X5 min with PBS, tissue sections were

25   coverslipped with Mowiol mounting medium. Coverslips were imaged using an Olympus

15

1 BX63 epifluorescence microscope equipped with SC50 camera for brightfield and XM10

2 camera for fluorescence.

4.5. Image analysis

4 Intracellular virus distribution was analyzed using a Leica TCS SP5 confocal microscope.

5 Individual cells among those that were in focal field were randomly chosen and the spatial

6 relationship between SARS-CoV-2 *ish* probe signal and cytoskeleton network (α-tubulin) was

7 visually assessed. For each condition, 20 infected cells were at least acquired. All of the images

8 were recorded at the same laser and multiplier settings.

9 For neurite length assessment, multiple representative brightfields of SH-SY5Y cells were

10 imaged using an inverted microscope Olympus CKX41 equipped with EP50 camera. The

11 channels were extracted to grey scale and the length of 5 to 10 neurites per field was traced and

12 measured, thereafter, from the distal end of neuron growth-cone, using the neurite tracer plugin

13 NeuronJ (ImageJ add-on software), according to published protocol (Pemberton et al., 2018).

14 From the images, at least 35 neurites per condition were quantified.

15 For the analysis of caspase-3 immunolabeling, 100 cells per experimental condition were

16 randomly acquired based on Hoescht nuclei counterstaining. The number of immunoreactive

17 cleaved caspase-3+ cells was manually and blinded counted, and further related to 100 cell

18 nuclei.

4.6. Glutamate Uptake Assay

20 The assay was adapted from Mahmoud et al. (Mahmoud et al., 2019). Briefly, 100,000 cells

21 were seeded in each well of a 96-well plate, and washed 2 times with Hank's Balanced Salt

22 Solution (HBSS) containing Ca^{2+} and Mg^{2+}: 1.26 mM $CaCl_2$, 5.36 mM KCl, 0.44 mM

23 KH_2PO_4, 0.811 mM $MgSO_4$, 137 mM NaCl, 0.336 mM Na_2HPO_4, 4.166 mM $NaHCO_3$, and

24 5.55 mM d-glucose. Cells were then incubated with HBSS containing 200 μM L-glutamic acid

25 (G-1251, Sigma-Aldrich, Overijse, BE) during 4 h. Culture supernatant was collected, and

16

1 glutamate concentration in the medium was measured using a glutamate colorimetric assay kit

2 according to the manufacturer's instructions (#MAK004, Sigma-Aldrich, Overijse, BE). Total

3 extracellular glutamate reflects the sum of glutamate uptake and release activities.

4 **4.7. Statistics**

5 Unless specified, all results were expressed as mean values ± Standard Error of Mean (SEM).

6 Mann–Whitney was used to assess statistical significance between two groups. For multiple

7 comparisons (≥3 groups), one-way non-parametric ANOVA test followed by Kruskal-Wallis

8 *post-hoc* analysis was used to compare each MOI condition. When groups had to be compared

9 based on two parameters (e.g. cell type and MOI), two-way non-parametric ANOVA test

10 followed by Dunnett's post-hoc analysis was used. The level of significance was set at $p<0.05$.

11 The statistical analyses were performed using the software GraphPad Prism version 7

12 (GraphPad Software, La Jolla, USA).

13

Gene name (accession number)	Primer sense 5'-3' Primer antisense 5'-3' [Taqman probe]	Product length (bp)
human *ace2* (NM_001371415.1)	5'-GGACCCAGGAAATGTTCAGA-3' 5'-GGCTGCAGAAAGTGACATGA-3'	238
human *tmprss2* (NM_001135099.1)	5'-CTGCCAAGGTGCTTCTCATT-3' 5'-CTGTCACCCTGGCAAGAATC-3'	127
human *ctsb* (NM_147783)	5'-AGAGTTATGTTTACCGAGGACCT-3' 5'-GATGCAGATCCGGTCAGAGA-3'	159
human *ctsl* (NM_145918)	5'-AAACTGGGAGGCTTATCTCACT-3' 5'-GCATAATCCATTAGGCCACCAT-3'	97
human *hprt* (NM_000194.3)	5'-TGACACTGGCAAAACAATGCA-3' 5'-GGTCCTTTTCACCAGCAAGCT-3'	94
SARS-CoV-2 *gene E* (NC_045512)	5'-ACAGGTACGTTAATAGTTAATAGCGT-3' 5'-ATATTGCAGCAGTACGCACACA-3' [(FAM)-ACACTAGCCATCCTTACTGCGCTTCG-(BHQ1)]	113

14 Table 1. Primer and probe sequences for qRT-PCR.

15

16

17

1   **Figure captions (ALL FIGURES IN COLOR)**

2   ~~Suppl.~~ **Figure~~.~~ 1.** Relative quantification of SARS-CoV-2 entry genes in human neural cell

3   lines: *ace2* and *tmprss2* (a); *ctsb* and *ctsl* (b). Ct cycles for entry genes were normalized to Ct

4   cycles of human *hprt* and relative expression data were expressed as 2e-ΔCt. Statistical

5   significance was assessed using Mann-Whitney only on SH-SY5Y and SK-N-BE(2) cells with

6   or without RA-based differentiation. *p<0.05. Each box plots the median and extends from the

7   25th to 75th percentiles. Whiskers shows the min. and max. values. n=4 independent samples

8   per condition.

9

10   **Figure ~~1~~2.** Chromogenic or fluorescent *in situ* hybridization (*ish*) using SARS-CoV-2 *gene S*

11   probe (nCoV2019-S, red) were applied on RA-differentiated SH-SY5Y and SK-N-BE(2) cells

12   exposed to SARS-CoV-2 at MOI 5.0 during 24 hours or to mock condition (a). Nuclei were

13   counterstained with Hoechst (blue). Scale bar represents 50 μm. Viral RNA was detected in the

14   cell body compartment of infected cells (black arrow) as well as along the neuritic processes

15   (black arrowheads). Scale bar represents 10 μm. In comparison, infection of epithelial VeroE6

16   cells with a lower MOI (0.1) of SARS-CoV-2 produced a massive *ish* signal in the cytoplasmic

17   compartment (upper right panel). Scale bar represents 20 μm. Quantification of SARS-CoV-2

18   *gene E* relative abundance in infected SH-SY5Y and SK-N-BE(2) according to various MOIs

19   and timings of infection (b). Ct cycles for *gene E* were normalized to Ct cycles of human *hprt*

20   and relative expression data were expressed as 2e-ΔCt. Statistical significance was calculated

21   using a two-way ANOVA comparing each MOI and each timing. *p<0.05; ***p<0.001 for

22   comparisons between each MOI, [###]p<0.001 for comparisons between 2 hours and 24 hours of

23   infection. n=3 independent samples for each condition. Representative multiplex nCoV2019S

24   *ish* (red)/ α-tubulin (green) immunofluorescence images showed that viral RNA was in the

25   same confocal plane as the cytoskeleton network in both infected neuroblastoma cell lines,

18

1   when cells were infected at MOI 5.0 during 24 hours (c). Scale bar represents 25 μm.

2   Orthogonal views from z-stack reconstruction confirmed the intracellular localization of SARS-

3   CoV-2 RNA signal. At 24 hours of infection, SARS-CoV-2 cytopathic effect was assessed by

4   measuring the length of neuritic processes grown by RA-differentiated SH-SY5Y cells (d).

5   Statistical significance was calculated using a one-way ANOVA comparing each MOI to mock

6   condition. N=35-39 neurites counted per condition. At 24 hours of infection, SARS-CoV-2

7   cytopathic effect was assessed by counting the number of cleaved caspase-3 immunoreactive

8   SH-SY5Y or SK-N-BE(2) cells, and compared to MOI-matched VeroE6 cells (e). Statistical

9   significance was calculated using a two-way ANOVA comparing each MOI and each cell type.

10   ***$p<0.001$ for comparisons between VeroE6 and SH-SY5Y or SK-N-BE(2), ##$p<0.01$,

11   ###$p<0.001$ for comparisons between MOI. N=100 cell nuclei counted per condition.

12   Abbreviations: MOI, multiplicity-of-infection; n.d., not detected; n.s., not significant.

13

14   **Figure ~~2~~3.** Chromogenic *in situ* hybridization (*ish*) using SARS-CoV-2 *gene S* probe

15   (nCoV2019-S) was applied on U-87 MG and U-373 MG cells exposed to SARS-CoV-2 at MOI

16   5.0 during 24 hours or to mock condition (a). Scale bar represents 20 μm. Viral RNA was

17   detected in the cell body compartment of infected cells as well as in the glial-like processes

18   (inset in the upper right panel). Quantification of SARS-CoV-2 *gene E* relative abundance in

19   infected SH-SY5Y and SK-N-BE(2) according to various MOIs and timings of infection (b).

20   Ct cycles for *gene E* were normalized to Ct cycles of human *hprt* and relative expression data

21   were expressed as 2e-ΔCt. Statistical significance was calculated using a two-way ANOVA

22   comparing each MOI and each timing. **$p<0.01$; ***$p<0.001$ for comparisons between each

23   MOI, ###$p<0.001$ for comparisons between 2 hours and 24 hours of infection. N=3 independent

24   samples for each condition. Representative multiplex nCoV2019S *ish* (red)/ GFAP (green)

19

immunofluorescence images showed SARS-CoV-2 abilities to infect both GFAP^{low}-expressing cells (U-87 MG) and GFAP^{high}-expressing cells (U-373 MG), upon infection with MOI 5.0 during 24 hours (c). Scale bar represents 20 μm. At 24 hours of infection, SARS-CoV-2 cytopathic effect was assessed by quantifying the ability of U-373 MG cells to take up extracellular glutamate added to the culture supernatant (200 μM) (d). Infected U-373 MG cells were able to pump up glutamate from supernatant as efficiently as non-infected cells (p=n.s.). Statistical significance was calculated using a one-way ANOVA comparing each MOI to mock condition. N=6 independent samples per condition. At 24 hours of infection, SARS-CoV-2 cytopathic effect was assessed by counting the number of cleaved caspase-3 immunoreactive U-87 MG or U-373 MG cells, and compared to MOI-matched VeroE6 cells (e). Statistical significance was calculated using a two-way ANOVA comparing each MOI and each cell type. ***p<0.001 for comparisons between VeroE6 and U-87 MG or U-373 MG, $^{##}$p<0.01, $^{###}$p<0.001 for comparisons between MOI. n=100 cell nuclei counted per condition. Abbreviations: MOI, multiplicity-of-infection; n.d., not detected; n.s., not significant.

~~**Suppl. Fig. 1.** Relative quantification of SARS-CoV-2 entry genes in human neural cell lines: *ace2* and *tmprss2* (a); *ctsb* and *ctsl* (b). Ct cycles for entry genes were normalized to Ct cycles of human *hprt* and relative expression data were expressed as 2e-ΔCt. Statistical significance was assessed using Mann-Whitney only on SH-SY5Y and SK-N-BE(2) cells with or without RA-based differentiation. *p<0.05. Each box plots the median and extends from the 25th to 75th percentiles. Whiskers shows the min. and max. values. n=4 independent samples per condition.~~

1 **Suppl. Fig. 21.** Representative confocal images of SARS-CoV-2 infected neuroblastoma cells,

2 labeled for nCoV2019-S (red), α-tubulin (green) and counterstained with Hoechst (blue nuclei).

3 Analysis of peak fluorescence intensity from one confocal plane shows the co-localization of

4 red and green peaks at several distances (asterix) along the region-of-interest.

5

Acknowledgments

Author contribution

Data curation, Formal analysis, Methodology: V.B., K.W., N.A., K.D, R.L., N.N.

Conceptualization, Writing – Original Draft Preparation: N.G., C.N.

Writing – Review & Editing: J.G., N.G.

Conflicts of Interest

The authors declare no conflict of interest.

Submission declaration

This manuscript has not been published or is being reviewed elsewhere.

References

Asadi-Pooya, A.A., Simani, L., 2020. Central nervous system manifestations of COVID-19: A systematic review. J Neurol Sci. 413**,** 116832.

Bulfamante, G., Chiumello, D., Canevini, M.P., Priori, A., Mazzanti, M., Centanni, S., Felisati, G., 2020. First ultrastructural autoptic findings of SARS -Cov-2 in olfactory pathways and brainstem. Minerva Anestesiol. 86**,** 678-679.

Bullen, C.K., Hogberg, H.T., Bahadirli-Talbott, A., Bishai, W.R., Hartung, T., Keuthan, C., Looney, M.M., Pekosz, A., Romero, J.C., Sillé, F.C.M., Um, P., Smirnova, L., 2020. Infectability of human BrainSphere neurons suggests neurotropism of SARS-CoV-2. Altex. 37**,** 665-671.

Cantuti-Castelvetri, L., Ojha, R., Pedro, L.D., Djannatian, M., Franz, J., Kuivanen, S., van der Meer, F., Kallio, K., Kaya, T., Anastasina, M., Smura, T., Levanov, L., Szirovicza, L., Tobi, A., Kallio-Kokko, H., Österlund, P., Joensuu, M., Meunier, F.A., Butcher, S.J., Winkler, M.S., Mollenhauer, B., Helenius, A., Gokce, O., Teesalu, T., Hepojoki, J., Vapalahti, O., Stadelmann, C., Balistreri, G., Simons, M., 2020. Neuropilin-1 facilitates SARS-CoV-2 cell entry and infectivity. Science. 370**,** 856-860.

Chen, N., Zhou, M., Dong, X., Qu, J., Gong, F., Han, Y., Qiu, Y., Wang, J., Liu, Y., Wei, Y., Xia, J., Yu, T., Zhang, X., Zhang, L., 2020. Epidemiological and clinical characteristics of 99 cases of 2019 novel coronavirus pneumonia in Wuhan, China: a descriptive study. Lancet. 395**,** 507-513.

Chu, H., Chan, J.F., Yuen, T.T., Shuai, H., Yuan, S., Wang, Y., Hu, B., Yip, C.C., Tsang, J.O., Huang, X., Chai, Y., Yang, D., Hou, Y., Chik, K.K., Zhang, X., Fung, A.Y., Tsoi, H.W., Cai, J.P., Chan, W.M., Ip, J.D., Chu, A.W., Zhou, J., Lung, D.C., Kok, K.H., To, K.K., Tsang, O.T., Chan, K.H., Yuen, K.Y., 2020. Comparative tropism, replication kinetics, and cell damage profiling of SARS-CoV-2 and SARS-CoV with implications for clinical manifestations, transmissibility, and laboratory studies of COVID-19: an observational study. Lancet Microbe. 1**,** e14-e23.

Coolen, T., Lolli, V., Sadeghi, N., Rovai, A., Trotta, N., Taccone, F.S., Creteur, J., Henrard, S., Goffard, J.C., De Witte, O., Naeije, G., Goldman, S., De Tiege, X., 2020. Early postmortem brain MRI findings in COVID-19 non-survivors. Neurology.

Coupeau, D., Burton, N., Lejeune, N., Loret, S., Petit, A., Pejakovic, S., Poulain, F., Bonil, L., Trozzi, G., Wiggers, L., Willemart, K., André, E., Laenen, L., Cuypers, L., Van Ranst, M., Bogaerts, P., Muylkens, B., Gillet, N.A., 2020. SARS-CoV-2 Detection for Diagnosis Purposes in the Setting of a Molecular Biology Research Lab. Methods Protoc. 3.

Gu, J., Gong, E., Zhang, B., Zheng, J., Gao, Z., Zhong, Y., Zou, W., Zhan, J., Wang, S., Xie, Z., Zhuang, H., Wu, B., Zhong, H., Shao, H., Fang, W., Gao, D., Pei, F., Li, X., He, Z., Xu, D., Shi, X., Anderson, V.M., Leong, A.S., 2005. Multiple organ infection and the pathogenesis of SARS. J Exp Med. 202**,** 415-24.

Gupta, A., Madhavan, M.V., Sehgal, K., Nair, N., Mahajan, S., Sehrawat, T.S., Bikdeli, B., Ahluwalia, N., Ausiello, J.C., Wan, E.Y., Freedberg, D.E., Kirtane, A.J., Parikh, S.A., Maurer, M.S., Nordvig, A.S., Accili, D., Bathon, J.M., Mohan, S., Bauer, K.A., Leon, M.B., Krumholz, H.M., Uriel, N., Mehra, M.R., Elkind, M.S.V., Stone, G.W., Schwartz, A., Ho, D.D., Bilezikian, J.P., Landry, D.W., 2020. Extrapulmonary manifestations of COVID-19. Nat Med. 26**,** 1017-1032.

Helms, J., Kremer, S., Merdji, H., Clere-Jehl, R., Schenck, M., Kummerlen, C., Collange, O., Boulay, C., Fafi-Kremer, S., Ohana, M., Anheim, M., Meziani, F., 2020. Neurologic Features in Severe SARS-CoV-2 Infection. N Engl J Med. 382**,** 2268-2270.

Hoffmann, M., Kleine-Weber, H., Schroeder, S., Krüger, N., Herrler, T., Erichsen, S., Schiergens, T.S., Herrler, G., Wu, N.H., Nitsche, A., Müller, M.A., Drosten, C., Pöhlmann, S.,

1 2020. SARS-CoV-2 Cell Entry Depends on ACE2 and TMPRSS2 and Is Blocked by a
2 Clinically Proven Protease Inhibitor. Cell. 181**,** 271-280.e8.
3 Kanberg, N., Ashton, N.J., Andersson, L.M., Yilmaz, A., Lindh, M., Nilsson, S., Price, R.W.,
4 Blennow, K., Zetterberg, H., Gisslén, M., 2020. Neurochemical evidence of astrocytic and
5 neuronal injury commonly found in COVID-19. Neurology. 95**,** e1754-e1759.
6 Kilinc, D., van de Pasch, S., Doets, A.Y., Jacobs, B.C., van Vliet, J., Garssen, M.P.J., 2020.
7 Guillain-Barré syndrome after SARS-CoV-2 infection. Eur J Neurol.
8 Kumari, P., Rothan, H.A., Natekar, J.P., Stone, S., Pathak, H., Strate, P.G., Arora, K., Brinton,
9 M.A., Kumar, M., 2021. Neuroinvasion and Encephalitis Following Intranasal Inoculation of
10 SARS-CoV-2 in K18-hACE2 Mice. Viruses. 13.
11 Lu, R., Zhao, X., Li, J., Niu, P., Yang, B., Wu, H., Wang, W., Song, H., Huang, B., Zhu, N.,
12 Bi, Y., Ma, X., Zhan, F., Wang, L., Hu, T., Zhou, H., Hu, Z., Zhou, W., Zhao, L., Chen, J.,
13 Meng, Y., Wang, J., Lin, Y., Yuan, J., Xie, Z., Ma, J., Liu, W.J., Wang, D., Xu, W., Holmes,
14 E.C., Gao, G.F., Wu, G., Chen, W., Shi, W., Tan, W., 2020. Genomic characterisation and
15 epidemiology of 2019 novel coronavirus: implications for virus origins and receptor binding.
16 Lancet. 395**,** 565-574.
17 Mahmoud, S., Gharagozloo, M., Simard, C., Gris, D., 2019. Astrocytes Maintain Glutamate
18 Homeostasis in the CNS by Controlling the Balance between Glutamate Uptake and Release.
19 Cells. 8.
20 Mao, L., Jin, H., Wang, M., Hu, Y., Chen, S., He, Q., Chang, J., Hong, C., Zhou, Y., Wang, D.,
21 Miao, X., Li, Y., Hu, B., 2020a. Neurologic Manifestations of Hospitalized Patients With
22 Coronavirus Disease 2019 in Wuhan, China. JAMA Neurol. 77**,** 683-690.
23 Mao, L., Wang, M., Chen, S., He, Q., Chang, J., Hong, C., Zhou, Y., Wang, D., Li, Y., Jin, H.,
24 Hu, B., 2020b. Neurological Manifestations of Hospitalized Patients with COVID-19 in
25 Wuhan, China: a retrospective case series study. medRxiv. 2020.02.22.20026500.
26 Meinhardt, J., Radke, J., Dittmayer, C., Franz, J., Thomas, C., Mothes, R., Laue, M., Schneider,
27 J., Brünink, S., Greuel, S., Lehmann, M., Hassan, O., Aschman, T., Schumann, E., Chua, R.L.,
28 Conrad, C., Eils, R., Stenzel, W., Windgassen, M., Rößler, L., Goebel, H.H., Gelderblom, H.R.,
29 Martin, H., Nitsche, A., Schulz-Schaeffer, W.J., Hakroush, S., Winkler, M.S., Tampe, B.,
30 Scheibe, F., Körtvélyessy, P., Reinhold, D., Siegmund, B., Kühl, A.A., Elezkurtaj, S., Horst,
31 D., Oesterhelweg, L., Tsokos, M., Ingold-Heppner, B., Stadelmann, C., Drosten, C., Corman,
32 V.M., Radbruch, H., Heppner, F.L., 2020. Olfactory transmucosal SARS-CoV-2 invasion as a
33 port of central nervous system entry in individuals with COVID-19. Nat Neurosci.
34 Moriguchi, T., Harii, N., Goto, J., Harada, D., Sugawara, H., Takamino, J., Ueno, M., Sakata,
35 H., Kondo, K., Myose, N., Nakao, A., Takeda, M., Haro, H., Inoue, O., Suzuki-Inoue, K.,
36 Kubokawa, K., Ogihara, S., Sasaki, T., Kinouchi, H., Kojin, H., Ito, M., Onishi, H., Shimizu,
37 T., Sasaki, Y., Enomoto, N., Ishihara, H., Furuya, S., Yamamoto, T., Shimada, S., 2020. A first
38 case of meningitis/encephalitis associated with SARS-Coronavirus-2. Int J Infect Dis. 94**,** 55-
39 58.
40 Netland, J., Meyerholz, D.K., Moore, S., Cassell, M., Perlman, S., 2008. Severe acute
41 respiratory syndrome coronavirus infection causes neuronal death in the absence of encephalitis
42 in mice transgenic for human ACE2. J Virol. 82**,** 7264-75.
43 Ortiz, M.E., Thurman, A., Pezzulo, A.A., Leidinger, M.R., Klesney-Tait, J.A., Karp, P.H., Tan,
44 P., Wohlford-Lenane, C., McCray, P.B., Jr., Meyerholz, D.K., 2020. Heterogeneous expression
45 of the SARS-Coronavirus-2 receptor ACE2 in the human respiratory tract. EBioMedicine. 60**,**
46 102976.
47 Paniz-Mondolfi, A., Bryce, C., Grimes, Z., Gordon, R.E., Reidy, J., Lednicky, J., Sordillo,
48 E.M., Fowkes, M., 2020. Central nervous system involvement by severe acute respiratory
49 syndrome coronavirus-2 (SARS-CoV-2). J Med Virol. 92**,** 699-702.

1 Paterson, R.W., Brown, R.L., Benjamin, L., Nortley, R., Wiethoff, S., Bharucha, T., Jayaseelan, D.L., Kumar, G., Raftopoulos, R.E., Zambreanu, L., Vivekanandam, V., Khoo, A., Geraldes, R., Chinthapalli, K., Boyd, E., Tuzlali, H., Price, G., Christofi, G., Morrow, J., McNamara, P., McLoughlin, B., Lim, S.T., Mehta, P.R., Levee, V., Keddie, S., Yong, W., Trip, S.A., Foulkes, A.J.M., Hotton, G., Miller, T.D., Everitt, A.D., Carswell, C., Davies, N.W.S., Yoong, M., Attwell, D., Sreedharan, J., Silber, E., Schott, J.M., Chandratheva, A., Perry, R.J., Simister, R., Checkley, A., Longley, N., Farmer, S.F., Carletti, F., Houlihan, C., Thom, M., Lunn, M.P., Spillane, J., Howard, R., Vincent, A., Werring, D.J., Hoskote, C., Jäger, H.R., Manji, H., Zandi, M.S., 2020. The emerging spectrum of COVID-19 neurology: clinical, radiological and laboratory findings. Brain. 143**,** 3104-3120.

2 Pemberton, K., Mersman, B., Xu, F., 2018. Using ImageJ to Assess Neurite Outgrowth in Mammalian Cell Cultures: Research Data Quantification Exercises in Undergraduate Neuroscience Lab. J Undergrad Neurosci Educ. 16**,** A186-a194.

3 Poyiadji, N., Shahin, G., Noujaim, D., Stone, M., Patel, S., Griffith, B., 2020. COVID-19-associated Acute Hemorrhagic Necrotizing Encephalopathy: CT and MRI Features. Radiology. 201187.

4 Puelles, V.G., Lütgehetmann, M., Lindenmeyer, M.T., Sperhake, J.P., Wong, M.N., Allweiss, L., Chilla, S., Heinemann, A., Wanner, N., Liu, S., Braun, F., Lu, S., Pfefferle, S., Schröder, A.S., Edler, C., Gross, O., Glatzel, M., Wichmann, D., Wiech, T., Kluge, S., Pueschel, K., Aepfelbacher, M., Huber, T.B., 2020. Multiorgan and Renal Tropism of SARS-CoV-2. N Engl J Med. 383**,** 590-592.

5 Radzikowska, U., Ding, M., Tan, G., Zhakparov, D., Peng, Y., Wawrzyniak, P., Wang, M., Li, S., Morita, H., Altunbulakli, C., Reiger, M., Neumann, A.U., Lunjani, N., Traidl-Hoffmann, C., Nadeau, K.C., O'Mahony, L., Akdis, C., Sokolowska, M., 2020. Distribution of ACE2, CD147, CD26, and other SARS-CoV-2 associated molecules in tissues and immune cells in health and in asthma, COPD, obesity, hypertension, and COVID-19 risk factors. Allergy. 75**,** 2829-2845.

6 Ramani, A., Müller, L., Ostermann, P.N., Gabriel, E., Abida-Islam, P., Müller-Schiffmann, A., Mariappan, A., Goureau, O., Gruell, H., Walker, A., Andrée, M., Hauka, S., Houwaart, T., Dilthey, A., Wohlgemuth, K., Omran, H., Klein, F., Wieczorek, D., Adams, O., Timm, J., Korth, C., Schaal, H., Gopalakrishnan, J., 2020. SARS-CoV-2 targets neurons of 3D human brain organoids. Embo j. 39**,** e106230.

7 Song, E., Zhang, C., Israelow, B., Lu-Culligan, A., Prado, A.V., Skriabine, S., Lu, P., Weizman, O.E., Liu, F., Dai, Y., Szigeti-Buck, K., Yasumoto, Y., Wang, G., Castaldi, C., Heltke, J., Ng, E., Wheeler, J., Alfajaro, M.M., Levavasseur, E., Fontes, B., Ravindra, N.G., Van Dijk, D., Mane, S., Gunel, M., Ring, A., Kazmi, S.A.J., Zhang, K., Wilen, C.B., Horvath, T.L., Plu, I., Haik, S., Thomas, J.L., Louvi, A., Farhadian, S.F., Huttner, A., Seilhean, D., Renier, N., Bilguvar, K., Iwasaki, A., 2021. Neuroinvasion of SARS-CoV-2 in human and mouse brain. J Exp Med. 218.

8 Uversky, V.N., Elrashdy, F., Aljadawi, A., Ali, S.M., Khan, R.H., Redwan, E.M., 2020. Severe acute respiratory syndrome coronavirus 2 infection reaches the human nervous system: How? J Neurosci Res.

9 Yang, L., Han, Y., Nilsson-Payant, B.E., Gupta, V., Wang, P., Duan, X., Tang, X., Zhu, J., Zhao, Z., Jaffré, F., Zhang, T., Kim, T.W., Harschnitz, O., Redmond, D., Houghton, S., Liu, C., Naji, A., Ciceri, G., Guttikonda, S., Bram, Y., Nguyen, D.T., Cioffi, M., Chandar, V., Hoagland, D.A., Huang, Y., Xiang, J., Wang, H., Lyden, D., Borczuk, A., Chen, H.J., Studer, L., Pan, F.C., Ho, D.D., tenOever, B.R., Evans, T., Schwartz, R.E., Chen, S., 2020. A Human Pluripotent Stem Cell-based Platform to Study SARS-CoV-2 Tropism and Model Virus Infection in Human Cells and Organoids. Cell Stem Cell. 27**,** 125-136.e7.

10 Ye, Z.C., Sontheimer, H., 1999. Glioma cells release excitotoxic concentrations of glutamate. Cancer Res. 59**,** 4383-91.

1 Zanin, L., Saraceno, G., Panciani, P.P., Renisi, G., Signorini, L., Migliorati, K., Fontanella,
2 M.M., 2020. SARS-CoV-2 can induce brain and spine demyelinating lesions. Acta Neurochir
3 (Wien). 162, 1491-1494.
4 Zhang, B.Z., Chu, H., Han, S., Shuai, H., Deng, J., Hu, Y.F., Gong, H.R., Lee, A.C., Zou, Z.,
5 Yau, T., Wu, W., Hung, I.F., Chan, J.F., Yuen, K.Y., Huang, J.D., 2020. SARS-CoV-2 infects
6 human neural progenitor cells and brain organoids. Cell Res. 30, 928-931.
7 Zhao, K., Huang, J., Dai, D., Feng, Y., Liu, L., Nie, S., 2020. Acute myelitis after SARS-CoV-
8 2 infection: a case report. medRxiv. 2020.03.16.20035105.
9

26

1

Susceptibility of neuroblastoma and glioblastoma cell lines

to SARS-CoV-2 infection

Valéry Bielarz[1], Kévin Willemart[2], Noémie Avalosse[1], Kathleen De Swert[1], Riselane Lotfi[1],

Noémie Lejeune[2], Florian Poulain[2], Noelle Ninanne[3], Jacques Gilloteaux[1,4], Nicolas Gillet[2],

Charles Nicaise[1]

[1] URPhyM, NARILIS, Université de Namur, Namur, Belgium

[2] URVI, Université de Namur, Namur, Belgium

[3] URBC, Université de Namur, Namur, Belgium

[4] Department of Anatomical Sciences, St George's University School of Medicine, Newcastle upon Tyne, United Kingdom

valery.bielarz@unamur.be; kevin.willemart@unamur.be; noemie.avalosse@student.unamur.be; kathleen.deswert@unamur.be; riselane.lotfi@student.unamur.be; noemie.lejeune@unamur.be; poulainflorian@gmail.com; noelle.ninanne@unamur.be; JGilloteaux@sgu.edu; nicolas.gillet@unamur.be; charles.nicaise@unamur.be

Correspondence to: Prof. Charles NICAISE

e-mail : charles.nicaise@unamur.be

Address: Université de Namur, URPhyM – NARILIS, Rue de Bruxelles 61, B-5000 Namur,

BELGIUM

Phone: +3281724256

Abstract (< 250 words)

1

1   Modelling cell infection in-a-dish can represent a useful tool to understand the susceptibility of

2   different cell types towards severe acute respiratory coronavirus-2 (SARS-CoV-2) and to

3   decipher its neurotropism. In this perspective, retinoic acid (RA)-differentiated neuroblastoma

4   cell lines, SH-SY5Y and SK-N-BE(2) and glioblastoma cell lines, U-87 MG and U-373 MG,

5   were infected with a SARS-CoV-2 strain, at various multiplicity-of-infection (MOI). We first

6   demonstrated that the common entry genes - needed for invading epithelial cells - were

7   expressed. RA-differentiation induced an upregulation of *ace2* and *tmprss2* gene expression

8   while inducing downregulation of *ctsb* and *ctsl*. Using *in situ* hybridization and confocal

9   analysis, SARS-CoV-2 *gene S* RNA was detected intracellularly at MOI 5.0, and localized in

10   both soma and neuritic-like or glial-like processes. The infection was confirmed by

11   quantification of viral *gene E* RNA and showed a dose-dependency, with few infected cells at

12   MOI 0.1. After 24 hours of infection, no cytopathic effect was observed in SH-SY5Y abilities

13   to maintain neuritic processes or in U-373 MG for the uptake of glutamate. Unlike the

14   permissive Vero E6 cells, no significant apoptosis death was detected following SARS-CoV-2

15   infection of neuroblastoma or glioblastoma cells. This study demonstrates the susceptibility of

16   neuronal- and glial-like cell lines towards SARS-CoV-2 infection at high MOIs. Once inside

17   the cells, the virus does not seem to rapidly replicate nor exert major cytopathic effect. Overall,

18   our results strengthen the idea that SARS-CoV-2 has a tropism for nervous cells that express

19   commonly described entry genes.

1   **Keyword**s

2   SARS-CoV-2, neuroblastoma, glioblastoma, neurotropism, cytopathic effect, susceptibility

3

4

5   **Abbreviations**

6   SARS-CoV   severe acute respiratory syndrome coronavirus

7   SARS-CoV-2   severe acute respiratory syndrome coronavirus-2

8   COVID-19   coronavirus disease 2019

9   ace2   angiotensin-converting enzyme 2

10   tmprss2   transmembrane protease, serine 2

11   ctsb   cathepsin B

12   ctsl   cathepsin L

13   MOI   multiplicity-of-infection

14   ish   *in situ* hybridization

15   hprt   hypoxanthine-guanine phosphoribosyltransferase

16   RA   retinoic acid

17   BBB   blood-brain barrier

18

19

20   **Highlights**

21   * Neuroblastoma and glioblastoma cells express SARS-CoV-2 entry genes

22   * Neuroblastoma and glioblastoma cell lines are susceptible to SARS-CoV-2 infection

23   * Viral RNA is detected intracellularly in both soma and cell's extensions

24   * SARS-CoV-2 does not exert cytopathic effect on neuroblastoma or glioblastoma cells

25

3

1   **1. Introduction**

2   Most of the time, the infection with severe acute respiratory syndrome coronavirus 2 (SARS-

3   CoV-2) causes respiratory symptoms, known as coronavirus disease 2019 (COVID-19),

4   although a minority of patients are at risk of developing a severe form with extrapulmonary

5   involvements (for review (Gupta et al., 2020)). Severely SARS-CoV-2-affected patients are

6   more likely to develop neurologic symptoms (e.g. headache, epilepsy, confusion, nausea and

7   vomiting) than patients with a mild form of COVID-19 (Asadi-Pooya and Simani, 2020; Mao

8   et al., 2020a; Paterson et al., 2020). Among the worst neurologic cases, viral encephalitis,

9   necrotizing encephalopathy, acute myelitis or Guillain-Barré syndrome were reported (Chen et

10 al., 2020; Kilinc et al., 2020; Mao et al., 2020a; Moriguchi et al., 2020; Poyiadji et al., 2020;

11 Zhao et al., 2020). Intriguingly, some patients developed neurologic symptoms even prior to

12 any respiratory manifestation. In one retrospective study, up to 88% among the severe patients

13 showed acute cerebrovascular diseases associated with impaired consciousness (Mao et al.,

14 2020b). Neuro-imaging supports substantial brain damages in both COVID-19 survivors and

15 non-survivors (Coolen et al., 2020; Helms et al., 2020; Zanin et al., 2020). Increasing evidences

16 show the presence of SARS-Cov-2 in brain *post-mortem* tissue (Bulfamante et al., 2020; Paniz-

17 Mondolfi et al., 2020; Puelles et al., 2020; Song et al., 2021), even though the mechanisms and

18 routes of CNS entry are still elusive.

19 SARS-CoV-2 belongs to the same beta-coronaviruses family as SARS-CoV (2003 China

20 outbreak) and shares up to 79,6% pairwise identities on a genomic level with its cousin (Lu et

21 al., 2020). SARS-CoV-2 also shares common entry mechanisms used to invade target cells,

22 including the binding of the spike (S) protein to human ACE2 receptor. S protein sequence was

23 found to be approximately 77% homologous between SARS-CoV-2 and SARS-CoV. SARS-

24 CoV-2 entry also depends on TMPRSS2 protease activity, which helps at ACE2 cleavage and

25 receptor-binding domain unmasking, a condition required for membrane fusion (Hoffmann et

1   al., 2020). Alternatively, cathepsin B or L may be able to substitute for TMPRSS2 in early

2   endosomes upon endocytosis. ACE2 and TMPRSS2 have been detected at high expression

3   levels in nasal, bronchial epithelium, as well as in alveolar epithelium (mostly type II

4   pneumocytes), which explains the central respiratory pathology (Ortiz et al., 2020). Previously,

5   neuro-invasion abilities of SARS-CoV have been firmly demonstrated on both patients and

6   experimental animal models (Gu et al., 2005; Netland et al., 2008). Evidence from transgenic

7   humanized ACE2 mice showed that SARS-CoV is able to enter the nervous system through the

8   neuro-olfactory epithelium. It is then carried along the olfactory nerve up to the olfactory bulb,

9   where it starts to spread to neighboring nervous cells (Netland et al., 2008). Similar SARS-

10   CoV-2 neurotropic properties and CNS entry routes are under investigation. Of note, infected

11   cells from the olfactory neuro-epithelium are suggested as gateways to central nervous system

12   invasion in some individuals with COVID-19 (Cantuti-Castelvetri et al., 2020; Meinhardt et al.,

13   2020). Such an entry route was demonstrated as plausible in transgenic humanized ACE2 mice

14   following experimental intranasal instillation of SARS-CoV-2 (Kumari et al., 2021).

15   So far, *in vitro* data showed the permissiveness of U-251 glioblastoma cell line to SARS-CoV-

16   2 infection (Chu et al., 2020). Recently, evidences from five independent groups converge to

17   show that human neural progenitor cells, grown either as neurospheres or as brain organoids,

18   are susceptible to SARS-CoV-2 infection (Bullen et al., 2020; Ramani et al., 2020; Song et al.,

19   2021; Yang et al., 2020; Zhang et al., 2020). In the present report, we aim at investigating the

20   susceptibility of neuroblastoma and glioblastoma cell lines towards SARS-CoV-2 infection.

21   These respective neuron-like and glial-like cells might represent useful tools to decipher the

22   entry, replication and cytopathic effect of SARS-CoV-2 in the CNS.

2. Results

Before infecting the various neural cell lines with a Belgian SARS-CoV-2 strain, we sought to

explore their expression level of entry genes, encoding proteins commonly needed by SARS-

CoV-2 for invading human host cells. The transcripts for *ace2* and *tmprss2* genes were detected

in both neuroblastoma (SH-SY5Y and SK-N-BE(2)) and both glioblastoma (U-87 MG and U-

373 MG) cells, however in lower amounts than those of *hprt* housekeeping gene (Figure 1a).

Interestingly, RA-driven neuronal differentiation in SH-SY5Y and SK-N-BE(2) induced a

significant upregulation of *ace2* mRNA, compared to undifferentiated cells

(0.0007197 ± 7.698e-005 *vs.* $0.003234\pm0,0005701$ in SH-SY5Y, $p<0.05$; 0.004433 ± 0.00107 *vs.*

0.01072 ± 0.001291 in SK-N-BE(2), $p<0.05$). Similarly, *tmprss2* gene expression was

significantly induced upon RA differentiation (0.0008177 ± 6.422e-005 *vs.*

0.005994 ± 0.0008207 in SH-SY5Y, $p<0.05$; 0.05964 ± 0.02418 *vs.* 0.1956 ± 0.008158 in SK-N-

BE(2), $p<0.05$, RA-differentiated cells *vs.* undifferentiated cells). No comparison was made

between cell lines due to variable amounts of *hprt* housekeeping gene. The transcripts of

cathepsin B and L were expressed at higher levels than *hprt* across all cell lines analyzed (Figure

1b). RA-induced differentiation produced a significant downregulation of *ctsb* mRNA in SK-

N-BE(2) cells (27.61 ± 2.809 *vs.* 21.35 ± 1.185, $p=0.05$). Additionally, RA-induced

differentiation produced a significant downregulation of *ctsl* mRNA in both SH-SY5Y and SK-

N-BE(2) (4.317 ± 0.8435 *vs.* 2.311 ± 0.1334, $p<0.05$; 10.99 ± 1.412 *vs.* 4.942 ± 0.4085, $p<0.05$, RA-

differentiated cells *vs.* undifferentiated cells).

RA-differentiated SH-SY5Y and SK-N-BE(2) were infected with SARS-CoV-2 at various

MOIs during 2 or 24 hours. Viral RNA was revealed using fluorescent or chromogenic *in situ*

hybridization (*ish*) targeting the *gene S*. After 24 hours at a MOI 5.0 of infection, *ish* signal was

visualized in the cell bodies (black arrow), and to a certain extent in the neuritic processes

(arrowheads in Figure 2a). At MOI 0.1 and 1.0, *ish* signal was much sparser, probably reflecting

1   a fewer number of infected neuroblastoma cells (data not shown). In comparison, infection of

2   highly permissive VeroE6 cells with a MOI of 0.1 during 24 hours produces a massive *ish*

3   signal in the cytoplasmic compartment (Figure 2a). The entry of viral particles in neuroblastoma

4   cell lines was quantified using a qRT-PCR targeting the SARS-CoV-2 *gene E* (Figure 2b). In

5   SH-SY5Y, a 24 hours infection with MOIs 1.0 and 5.0 produced a significant amplification of

6   SARS-CoV-2 RNA from lyzed cells, in a dose-dependent manner (respectively 1.398±0.0976,

7    $p<0.05$; 10.73±0.7595, $p<0.001$ when compared to mock condition). Noteworthy, the relative

8   amount of *gene E* detected was higher when SH-SY5Y cells were infected at MOI 5.0 for 24

9   hours than for 2 hours (10.73±0.7595 vs. 5.713±0.1542, $p<0.001$). In SK-N-BE(2) cells, only

10   the highest MOI produced a significant infection at both timings, when compared to mock

11   condition (respectively 1.443±0.4262, $p<0.001$ and 1.284±0.09506, $p<0.001$). No difference of

12   viral RNA amount was observed between 2 hours and 24 hours of infection. Given that neither

13   transmitted light microscopy or qRT-PCR assays could provide a definitive answer about the

14   viral entry – i.e. viral particles could be adsorbed at the cell surface non-specifically or receptor-

15   bound – into host cells, we assessed the intracellular localization of viral RNA by confocal

16   analysis.   The cytoskeleton of SH-SY5Y and SK-N-BE(2) cells was visualized using

17   immunofluorescence against α-tubulin while SARS-CoV-2 gene S was revealed using

18   fluorescent *ish* (Figure 2c). In both cell lines, viral RNA was found in the same confocal plane

19   as α-tubulin network. Further analysis of fluorescence intensity confirmed that fluorescent

20   peaks, corresponding to SARS-CoV-2 gene S (red) and to α-tubulin (green), were overlapping

21   (asterix in Suppl. Fig. 1).

22   We next investigated a cytopathic effect of SARS-CoV-2 once inside the cells by measuring

23   the length of neuritic processes grown by RA-differentiated SH-SY5Y (Figure 2d). No effect

24   of SARS-CoV-2 infection was observed on the abilities of differentiated SH-SY5Y cells to

25   maintain their neurites, even at the highest MOI of 5.0 after 24 hours of infection (52.72±2.167

1   µm compared to 52.98±2.037 µm in mock condition, p=n.s.). In the same line, we sought to

2   know whether SARS-CoV-2 could induce cell death in infected nervous cell lines. The

3   apoptosis rate was quantified in VeroE6 cells and compared to infected SH-SY5Y and SK-N-

4   BE(2) cells (Figure 2e). While VeroE6 cells are highly permissive to SARS-CoV-2 (Figure 2a)

5   and are therefore used to amplify the virus, many of infected cells undergo apoptosis-mediated

6   cell death upon replication and/or release of viral particles. In VeroE6, the number of cleaved

7   caspase-3 immunoreactive cells reached up to 25.33±2.603 % upon exposure to MOI 5.0 during

8   24 hours, compared to 2.000±0.5774 % in mock condition (p<0.001). Interestingly, neither SH-

9   SY5Y or SK-N-BE(2) showed overt apoptosis upon infection with SARS-CoV-2, at any MOIs

10   tested. For instance, the percentages of apoptotic cells were respectively 3.66±2.66 % and

11   7.00±4.04 % at MOI 5.0 in SH-SY5Y and SK-N-BE(2) (p=n.s., compared to 2.50±0.88 % in

12   mock conditions). Overall, both neuroblastoma cell lines were much less prone to apoptosis

13   than VeroE6 cells at comparable MOIs (two-way ANOVA, VeroE6 *vs.* SH-SY5Y:

14   $F_{(1,16)}$=44.21, p<0.001; VeroE6 *vs.* SK-N-BE(2) : $F_{(1,16)}$=30.61, p<0.001).

15   In order to evaluate the susceptibility of neural cell lines closer to a glial phenotype, U-87 MG

16   and U-373 MG glioblastoma cell lines were infected with SARS-CoV-2 according to the same

17   paradigm as neuroblastoma cells. At 2- or 24-hours post-infection, viral RNA was revealed

18   using chromogenic *in situ* hybridization targeting the *gene S* (Figure 3a). Following 24 hours

19   at MOI 5.0, infected cells showed obvious *ish* chromogenic deposits in the cell bodies as well

20   as in the glial-like processes (inset in Figure 2a). The entry of viral particles in glioblastoma

21   cells was also quantified using qRT-PCR (Figure 3b). In U-87 MG cells, a 24-hour infection

22   produced a significant amplification of SARS-CoV-2 RNA, in a dose-dependent manner

23   (0.323±0.05743 for MOI 1.0, p<0.01 and 1.125±0.07618 for MOI 5.0, p<0.001 compared to

24   mock condition). Even though the levels of infection followed a similar profile at 2 hours post-

25   infection, the relative amount of SARS-CoV-2 *gene E* was significantly lower at 24 hours than

1   at 2 hours of infection for MOI 5.0 (1.125±0.07618 vs. 1.617±0.1079, p<0.001). In U-373 MG,

2   only the highest MOI at 2 hours of infection led to a significant detection of viral RNA,

3   compared to mock condition (2.117±0.2568 *vs.* 0.0±0.0 undetected, p<0.001) (Figure 3b). A

4   24-hour infection produced a significant amplification in a dose-dependent manner

5   (0.9433±0.0382 for MOI 1.0, p<0.01 and 3.671±0.4731 for MOI 5.0, p<0.001 compared to

6   mock condition). At MOI 5.0, a longer infection time led to increased amount of *gene E*

7   detected in U-373 MG (2.117±0.2568 at 2 hours vs. 3.671±0.4731 at 24 hours, p<0.001).

8   U-87 and U-373 cell lines are both considered as glioblastoma cells comprising a heterogeneous

9   mixture of morphologically, biochemically and functionally distinct cancer cells. For instance,

10   they are both classified as astrocytoma cells but differ in terms of GFAP expression. Grown on

11   uncoated plastic culture dishes, U-87 MG cells are GFAP^{low} expressing cells whereas U-373

12   MG cells are GFAP^{high}-expressing cells (Figure 3c). Both cell lines, no matter they express

13   low or high GFAP levels, are susceptible to SARS-CoV-2 infection. U-87 and U-373 also differ

14   in glutamate uptake abilities, even though all glioma cell lines showed impaired glutamate

15   uptake compared to normal human astrocytes (Ye and Sontheimer, 1999). While U-87 cells

16   have lost this ability (data not shown), U-373 MG cells internalized glutamate upon addition of

17   200 μM of glutamate in the medium (111.4±3.452 μM compared to 224.7±8.722 μM in basal

18   medium without cells, p<0.001) (Figure 3d). Infection with various MOIs of SARS-CoV-2

19   during 24 hours did not impact U-373 cells in their glutamate uptake abilities (one-way

20   ANOVA, p= 0.4668 mock *vs.* MOI 0.1; p=0.0955 mock *vs.* MOI 1.0; p=0.9664 mock *vs.* MOI

21   5.0). Finally, SARS-CoV-2 cytopathic effect on glioblastoma cells was evaluated by counting

22   the number of cleaved caspase-3 positive cells at 24 hours of infection (Figure 3e). Infected U-

23   87 or U-373 did not show more apoptosis at any MOI tested than mock condition. For instance,

24   the percentages of apoptotic cells were respectively 5.00±3.60% and 8.33±0.88 % at MOI 5.0

1   in U-87 and U-373 (p=n.s., compared to 2.83±0.83 % in mock conditions). Overall,

2   glioblastoma cell lines were much less prone to apoptotic cell death than VeroE6 cells at

3   comparable MOIs (two-way ANOVA, VeroE6 *vs.* U-87 MG: $F_{(1,16)}$=38.70, p<0.001; VeroE6

4   *vs.* U-373 MG : $F_{(1,16)}$=38.78, p<0.001).

5

6

7

3. Discussion

Our main findings are that SARS-CoV-2 is able to invade neuroblastoma and glioblastoma cell lines, without exerting major cytopathic effect on either neuron-like morphology or on functional glutamate uptake, and without inducing obvious apoptosis. Although the viral entry-dependency on common entry genes was not investigated, a basal expression of ace2, tmprss2, cathepsin B and cathepsin L transcripts was detected in all cell lines. Noteworthy, RA-differentiated neuroblastoma cells upregulated the gene expression of surface receptors such as ace2 and tmprss2. The definitive entry mechanisms inside nervous cells are still debated and existence of alternative surface receptors that might be hijacked cannot be ruled out, as it is described for SARS-CoV and some epithelial cells or immune cells e.g. CD147/BSG, CD26/DPP4 (Radzikowska et al., 2020).

Our experimental design allows to conclude that neuroblastoma and glioblastoma cells are modestly susceptible to SARS-CoV-2 infection, based on the high MOI needed to infect cells. In comparison to recent studies, human brain organoids and neurospheres were respectively infected with MOIs of 10.0 and 0.1 (Bullen et al., 2020; Zhang et al., 2020). At early infection timings (24h), neuroblastoma and glioblastoma cells were not as permissive as VeroE6 epithelial cells. So far, contradictory results are reported about the SARS-CoV-2 replication into human neurons. While one study showed that SARS-CoV-2 entered neurons from brain organoids but did not replicate (Ramani et al., 2020), in two studies genomic viral material was found in the supernatant at higher level several hours post-infection than at the time zero of infection, which supports the release of new viral particles (Bullen et al., 2020; Zhang et al., 2020). Intriguingly, we did not observe major SARS-CoV-2 cytopathic effect on any cell lines, unlike what was described in infected brain neurospheres or despite the evidences of neuronal and astrocytic injury in COVID-19 patients (Kanberg et al., 2020; Ramani et al., 2020). This

1   might be explained by a better resistance of tumor cell lines towards SARS-CoV-2 infection or

2   a too short timing for apoptosis analysis.

3   Bearing in mind the limitation that *in situ* hybridization – and not immunofluorescence nor

4   electron microscopy - was used throughout this study to detect SARS-CoV-2, our confocal

5   images comforted the intracellular localization of viral RNA. Interestingly, viral RNA was

6   distributed in both soma, and neuron-like or glial-like extensions. So far, we did not investigate

7   whether this distribution was due to random internalization along the cell membrane or whether

8   internalized viral particles were able to be transported inside/along the cell processes. This last

9   concept is relevant for deciphering the CNS entry routes. Among the entry pathways, the

10 retrograde transport along nerve fibers from peripheral infected tissues (i.e. nasal cavity) or the

11 hematogenous pathway across the blood-brain barrier (BBB) are being demonstrated

12 (Meinhardt et al., 2020; Uversky et al., 2020). From our images showing SARS-CoV-2 RNA

13 in the cell processes, it is tempting to hypothesize that neuron-like or glial-like cells might

14 internalize viral particles at their farthest cell extension and then, using intracellular trafficking,

15 carry them back to the soma. Corollary, SARS-CoV-2 might penetrate the CNS gate by first

16 invading brain endothelial cells or following BBB disruption, then being caught at the

17 perivascular astrocytic processes (Uversky et al., 2020). This hypothesis is supported by

18 ultrastructural findings from autopsied COVID-19 patients, where authors captured viral

19 particles at the endothelial-astrocyte interface (Bulfamante et al., 2020; Paniz-Mondolfi et al.,

20 2020). This passage would even be eased in the context of an important systemic inflammation

21 that includes cytokines known to compromise BBB integrity (Uversky et al., 2020).

22 This study on SARS-CoV-2 cell tropism is complementary to those using human pluripotent

23 stem cell-based platform (Yang et al., 2020). Infection of neuroblastoma or glioblastoma cells

24 might serve as an easy and low-cost model for testing drugs that interfere with viral entry, e.g.

25 ACE2 neutralizing antibodies, or other viral life cycle targets.

1   **4. Experimental Procedure**

2   **4.1. Cell culture**

3   The SH-SY5Y neuroblastoma cell line, U-87 MG and U-373 MG glioblastoma cell lines were

4   kindly provided by Profs. Jean-Pierre Brion and Karelle Leroy (Université Libre de Bruxelles,

5   BE). The SK-N-BE(2) neuroblastoma cell line was a kind gift from Prof. Marielle Boonen

6   (Université de Namur, BE). All cell lines were used between passage 15 and 25. They were

7   maintained in DMEM/F12 (Life Technologies, Grand Island, NY, USA) supplemented with 10

8   % fetal bovine serum (Sigma-Aldrich, Overijse, BE) and penicillin/streptomycin (Sigma-

9   Aldrich, Overijse, BE / Millipore, USA). Cells were grown in a sterile incubator at 37 °C, 95

10   % air humidity and 5 % CO_2 concentration. Culture medium was changed twice a week,

11   depending on cell density, and cells were passaged for further cultivation or differentiation

12   experiment at 80 − 90 % confluency. For passaging, cells were trypsinized using 0.05 %

13   Trypsin/EDTA during 2 minutes, washed in medium and spun down at 130 g for 7 minutes and

14   further split at a ratio 1:10. For differentiation experiment, SH-SY5Y and SK-N-BE(2) cells

15   were seeded at a density of 20,000 cells per cm2, on glass coverslips pre-coated with 0.1 mg/ml

16   Poly-L-lysine (Sigma-Aldrich, Overijse, BE). A differentiation protocol was applied based on

17   7 day-exposure to 10 µM all-trans-retinoic acid (RA) (Sigma-Aldrich, Overijse, BE) added in

18   low-serum medium (DMEM/F12 + 2% FBS + penicillin/streptomycin). RA-driven

19   differentiation was initiated 24 h after seeding and fresh medium was replaced everyday up to

20   day 7. Vero cells, clone E6 (VeroE6), were used to amplify a purified SARS-CoV-2 strain

21   isolated from a Belgian COVID-19 patient.

22   **4.2. Infection with SARS-CoV-2**

23   All infections or viral amplification were performed in a biosafety level-3 laboratory

24   (Université de Namur, BE). The SARS-CoV-2 isolate was kindly provided by Prof. Piet Maes

25   (KULeuven, BE). The viral titer of SARS-CoV-2 strain was determined by TCID50 on culture

1   supernatant from infected Vero E6 cells. Neuroblastoma or glioblastoma cells were plated at a

2   density of 20,000 cells per cm2 in a 24-well plate for *in situ* hybridization or a 12-well plate for

3   gene expression studies. Cells were infected during 2- or 24- hours using a multiplicity-of-

4   infection (MOI) of 0.1, 1.0 or 5.0 in low-serum medium. For mock condition, cells were

5   incubated with the low-serum medium-only. At the end of infection, culture medium was

6   carefully discarded. Cells were thoroughly washed three times with PBS and either lyzed in

7   TriZol or chemically-fixed with 4% paraformaldehyde, ensuring virus inactivation.

4.3. RNA isolation and qRT-PCR

9   Cells were homogenized in 1 mL of Trizol reagent and total RNA was further isolated according

10   to manufacturer's instructions (Life Technologies, Bleiswijk, NL). RNA concentrations were

11   measured using a spetrophotometer Nanodrop 1000 (Thermo Scientific, Bleiswijk, NL). Total

12   RNAs (1µg), including viral and human RNAs, were reverse-transcribed using the Super Script

13   II RNase H reverse transcriptase kit according to manufacturer's instructions (Invitrogen,

14   Merelbeke, BE). cDNA was used to amplify SARS-CoV-2 *gene E* with Takyon Taqman kit

15   and human genes with Takyon SYBR Green kit (Eurogentec, Liège, BE) in a Light Cycler 96

16   device (Roche Diagnostics, Mannheim, DE) (Coupeau et al., 2020). Primer sequences are listed

17   in Table 1. Relative gene expression was computed using the ΔCq method with *hprt* as

18   housekeeping gene.

4.4. *in situ* hybridization and immunofluorescence

20   Coverslips were fixed in cold 4% paraformaldehyde during 20 minutes and then washed and

21   stored in PBS at 4°C. Fixed cells were used within one-week post-fixation. Expression of

22   SARS-CoV-2 *gene S* was detected according to manufacturer's kit instructions (RNAScope,

23   Advanced Cell Diagnostics, Bio-techne, Abingdon, UK) and by using a specific target probe

24   (RNAscope Probe-V-nCoV2019-S, #848561, Bio-techne, Abingdon, UK). Briefly, cells were

25   permeabilized with PBS plus 0.1% Tween 20 for 10 min. After washing, endogenous

1 peroxidases were blocked with hydrogen peroxide for 10 min followed by 2 washes in PBS.

2 Cells were then incubated with RNAScope® Protease III (Advanced Cell Diagnostics Inc,

3 Hayward, USA) for 10 min. and subsequently washed in PBS. Samples were incubated with

4 the probe specifically targeting SARS-CoV-2 *gene S* mRNA (RNAScope, #422511, Advanced

5 Cell Diagnostics, Bio-techne, Abingdon, UK) for 2 hours at 40°C and then washed for 2min in

6 RNAScope® wash buffer (Advanced Cell Diagnostics, Bio-techne, Abingdon, UK).

7 Amplification rounds 1-6 alternated from 30 to 15 min at 40°C. Between each amplification

8 round, samples were washed with RNAScope® wash buffer. Detection of probe signals was

9 performed by incubating samples with alkaline phosphatase (solution of RNAScope® Fast B

10 and A ratio 1:60) for 10 min. at room temperature. Samples were then washed in milliQ water.

11 Following *ish*, samples were either counterstained with hematoxylin (Sigma-Aldrich, Overijse,

12 BE), dried for 30 min. at 60°C and mounted using VectaMount® (Vector Laboratories,

13 Burlingame, USA) or fluorescently stained according to the protocol below.

14 For *ish*/immunofluorescence multiplexing, coverslips were further washed 5 min at RT in PBS.

15 Non-specific binding was blocked in a PBS-BSA 1% for 30min at RT. Then, samples were

16 incubated with primary antibodies in PBS-BSA 1 % buffer overnight at RT: α-tubulin (1:500,

17 T-5168, Sigma-Aldrich); GFAP (1:1000, G-3893, Sigma-Aldrich); cleaved caspase-3 (1:1000,

18 #9664, Cell Signaling). After that, samples were washed 3X5 min with PBS-BSA 1%.

19 Fluorophore-coupled secondary antibodies alexa fluor® 488 goat anti-mouse IgG 1:200

20 (#A11001, Life Technologies, Oregon, USA) or goat anti-rabbit IgG 1:200 (#A11008, Life

21 Technologies, Oregon, USA) in PBS-BSA1% were applied on their respective tissue sections

22 and incubated for 30 min at RT. Afterwards, they were washed 3X5 min with PBS-BSA 1%

23 and cell nuclei were stained in a solution of Hoechst 33258 (Life Technologies, Oregon, USA).

24 Finally, after 1X5 min wash with PBS-BSA 1% and 2X5 min with PBS, tissue sections were

25 coverslipped with Mowiol mounting medium. Coverslips were imaged using an Olympus

15

1   BX63 epifluorescence microscope equipped with SC50 camera for brightfield and XM10

2   camera for fluorescence.

3   **4.5. Image analysis**

4   Intracellular virus distribution was analyzed using a Leica TCS SP5 confocal microscope.

5   Individual cells among those that were in focal field were randomly chosen and the spatial

6   relationship between SARS-CoV-2 *ish* probe signal and cytoskeleton network (α-tubulin) was

7   visually assessed. For each condition, 20 infected cells were at least acquired. All of the images

8   were recorded at the same laser and multiplier settings.

9   For neurite length assessment, multiple representative brightfields of SH-SY5Y cells were

10   imaged using an inverted microscope Olympus CKX41 equipped with EP50 camera. The

11   channels were extracted to grey scale and the length of 5 to 10 neurites per field was traced and

12   measured, thereafter, from the distal end of neuron growth-cone, using the neurite tracer plugin

13   NeuronJ (ImageJ add-on software), according to published protocol (Pemberton et al., 2018).

14   From the images, at least 35 neurites per condition were quantified.

15   For the analysis of caspase-3 immunolabeling, 100 cells per experimental condition were

16   randomly acquired based on Hoescht nuclei counterstaining. The number of immunoreactive

17   cleaved caspase-3+ cells was manually and blinded counted, and further related to 100 cell

18   nuclei.

19   **4.6. Glutamate Uptake Assay**

20   The assay was adapted from Mahmoud et al. (Mahmoud et al., 2019). Briefly, 100,000 cells

21   were seeded in each well of a 96-well plate, and washed 2 times with Hank's Balanced Salt

22   Solution (HBSS) containing Ca^{2+} and Mg^{2+}: 1.26 mM $CaCl_2$, 5.36 mM KCl, 0.44 mM

23   KH_2PO_4, 0.811 mM $MgSO_4$, 137 mM NaCl, 0.336 mM Na_2HPO_4, 4.166 mM $NaHCO_3$, and

24   5.55 mM d-glucose. Cells were then incubated with HBSS containing 200 μM L-glutamic acid

25   (G-1251, Sigma-Aldrich, Overijse, BE) during 4 h. Culture supernatant was collected, and

1   glutamate concentration in the medium was measured using a glutamate colorimetric assay kit

2   according to the manufacturer's instructions (#MAK004, Sigma-Aldrich, Overijse, BE). Total

3   extracellular glutamate reflects the sum of glutamate uptake and release activities.

4   **4.7. Statistics**

5   Unless specified, all results were expressed as mean values ± Standard Error of Mean (SEM).

6   Mann–Whitney was used to assess statistical significance between two groups. For multiple

7   comparisons ($\geq$3 groups), one-way non-parametric ANOVA test followed by Kruskal-Wallis

8   *post-hoc* analysis was used to compare each MOI condition. When groups had to be compared

9   based on two parameters (e.g. cell type and MOI), two-way non-parametric ANOVA test

10 followed by Dunnett's post-hoc analysis was used. The level of significance was set at $p<0.05$.

11 The statistical analyses were performed using the software GraphPad Prism version 7

12 (GraphPad Software, La Jolla, USA).

13

Gene name (accession number)	Primer sense 5'-3' Primer antisense 5'-3' [Taqman probe]	Product length (bp)
human *ace2* (NM_001371415.1)	5'-GGACCCAGGAAATGTTCAGA-3' 5'-GGCTGCAGAAAGTGACATGA-3'	238
human *tmprss2* (NM_001135099.1)	5'-CTGCCAAGGTGCTTCTCATT-3' 5'-CTGTCACCCTGGCAAGAATC-3'	127
human *ctsb* (NM_147783)	5'-AGAGTTATGTTTACCGAGGACCT-3' 5'-GATGCAGATCCGGTCAGAGA-3'	159
human *ctsl* (NM_145918)	5'-AAACTGGGAGGCTTATCTCACT-3' 5'-GCATAATCCATTAGGCCACCAT-3'	97
human *hprt* (NM_000194.3)	5'-TGACACTGGCAAAACAATGCA-3' 5'-GGTCCTTTTCACCAGCAAGCT-3'	94
SARS-CoV-2 *gene E* (NC_045512)	5'-ACAGGTACGTTAATAGTTAATAGCGT-3' 5'-ATATTGCAGCAGTACGCACACA-3' [(FAM)-ACACTAGCCATCCTTACTGCGCTTCG-(BHQ1)]	113

14 Table 1. Primer and probe sequences for qRT-PCR.

15

16

17

1   **Figure captions (ALL FIGURES IN COLOR)**

2   **Figure 1.** Relative quantification of SARS-CoV-2 entry genes in human neural cell lines: *ace2*

3   and *tmprss2* (a); *ctsb* and *ctsl* (b). Ct cycles for entry genes were normalized to Ct cycles of

4   human *hprt* and relative expression data were expressed as 2e-ΔCt. Statistical significance was

5   assessed using Mann-Whitney only on SH-SY5Y and SK-N-BE(2) cells with or without RA-

6   based differentiation. *p<0.05. Each box plots the median and extends from the 25th to 75th

7   percentiles. Whiskers shows the min. and max. values. n=4 independent samples per condition.

8

9   **Figure 2.** Chromogenic or fluorescent *in situ* hybridization (*ish*) using SARS-CoV-2 *gene S*

10   probe (nCoV2019-S, red) were applied on RA-differentiated SH-SY5Y and SK-N-BE(2) cells

11   exposed to SARS-CoV-2 at MOI 5.0 during 24 hours or to mock condition (a). Nuclei were

12   counterstained with Hoechst (blue). Scale bar represents 50 μm. Viral RNA was detected in the

13   cell body compartment of infected cells (black arrow) as well as along the neuritic processes

14   (black arrowheads). Scale bar represents 10 μm. In comparison, infection of epithelial VeroE6

15   cells with a lower MOI (0.1) of SARS-CoV-2 produced a massive *ish* signal in the cytoplasmic

16   compartment (upper right panel). Scale bar represents 20 μm. Quantification of SARS-CoV-2

17   *gene E* relative abundance in infected SH-SY5Y and SK-N-BE(2) according to various MOIs

18   and timings of infection (b). Ct cycles for *gene E* were normalized to Ct cycles of human *hprt*

19   and relative expression data were expressed as 2e-ΔCt. Statistical significance was calculated

20   using a two-way ANOVA comparing each MOI and each timing. *p<0.05; ***p<0.001 for

21   comparisons between each MOI, [###]p<0.001 for comparisons between 2 hours and 24 hours of

22   infection. n=3 independent samples for each condition. Representative multiplex nCoV2019S

23   *ish* (red)/ α-tubulin (green) immunofluorescence images showed that viral RNA was in the

24   same confocal plane as the cytoskeleton network in both infected neuroblastoma cell lines,

25   when cells were infected at MOI 5.0 during 24 hours (c). Scale bar represents 25 μm.

1   Orthogonal views from z-stack reconstruction confirmed the intracellular localization of SARS-

2   CoV-2 RNA signal. At 24 hours of infection, SARS-CoV-2 cytopathic effect was assessed by

3   measuring the length of neuritic processes grown by RA-differentiated SH-SY5Y cells (d).

4   Statistical significance was calculated using a one-way ANOVA comparing each MOI to mock

5   condition. N=35-39 neurites counted per condition. At 24 hours of infection, SARS-CoV-2

6   cytopathic effect was assessed by counting the number of cleaved caspase-3 immunoreactive

7   SH-SY5Y or SK-N-BE(2) cells, and compared to MOI-matched VeroE6 cells (e). Statistical

8   significance was calculated using a two-way ANOVA comparing each MOI and each cell type.

9   ***$p < 0.001$ for comparisons between VeroE6 and SH-SY5Y or SK-N-BE(2), ##$p < 0.01$,

10   ###$p < 0.001$ for comparisons between MOI. N=100 cell nuclei counted per condition.

11   Abbreviations: MOI, multiplicity-of-infection; n.d., not detected; n.s., not significant.

12

13   **Figure 3.** Chromogenic *in situ* hybridization (*ish*) using SARS-CoV-2 *gene S* probe

14   (nCoV2019-S) was applied on U-87 MG and U-373 MG cells exposed to SARS-CoV-2 at MOI

15   5.0 during 24 hours or to mock condition (a). Scale bar represents 20 μm. Viral RNA was

16   detected in the cell body compartment of infected cells as well as in the glial-like processes

17   (inset in the upper right panel). Quantification of SARS-CoV-2 *gene E* relative abundance in

18   infected SH-SY5Y and SK-N-BE(2) according to various MOIs and timings of infection (b).

19   Ct cycles for *gene E* were normalized to Ct cycles of human *hprt* and relative expression data

20   were expressed as 2e-ΔCt. Statistical significance was calculated using a two-way ANOVA

21   comparing each MOI and each timing. **$p < 0.01$; ***$p < 0.001$ for comparisons between each

22   MOI, ###$p < 0.001$ for comparisons between 2 hours and 24 hours of infection. N=3 independent

23   samples for each condition. Representative multiplex nCoV2019S *ish* (red)/ GFAP (green)

24   immunofluorescence images showed SARS-CoV-2 abilities to infect both GFAP[low]-

1   expressing cells (U-87 MG) and GFAP^{high}-expressing cells (U-373 MG), upon infection with

2   MOI 5.0 during 24 hours (c). Scale bar represents 20 μm. At 24 hours of infection, SARS-CoV-

3   2 cytopathic effect was assessed by quantifying the ability of U-373 MG cells to take up

4   extracellular glutamate added to the culture supernatant (200 μM) (d). Infected U-373 MG cells

5   were able to pump up glutamate from supernatant as efficiently as non-infected cells (p=n.s.).

6   Statistical significance was calculated using a one-way ANOVA comparing each MOI to mock

7   condition. N=6 independent samples per condition. At 24 hours of infection, SARS-CoV-2

8   cytopathic effect was assessed by counting the number of cleaved caspase-3 immunoreactive

9   U-87 MG or U-373 MG cells, and compared to MOI-matched VeroE6 cells (e). Statistical

10   significance was calculated using a two-way ANOVA comparing each MOI and each cell type.

11   ***p<0.001 for comparisons between VeroE6 and U-87 MG or U-373 MG, $^{##}$p<0.01,

12    $^{###}$p<0.001 for comparisons between MOI. n=100 cell nuclei counted per condition.

13   Abbreviations: MOI, multiplicity-of-infection; n.d., not detected; n.s., not significant.

14

15

16   **Suppl. Fig. 1.** Representative confocal images of SARS-CoV-2 infected neuroblastoma cells,

17   labeled for nCoV2019-S (red), α-tubulin (green) and counterstained with Hoechst (blue nuclei).

18   Analysis of peak fluorescence intensity from one confocal plane shows the co-localization of

19   red and green peaks at several distances (asterix) along the region-of-interest.

20

1   **Acknowledgments**

2   We acknowledge Dr. Piet MAES (KUL, Belgium) for the kind gift of the purified

3   SARS-CoV-2 strain isolated from a Belgian COVID-19 patient. We are grateful to Prof.

4   Xavier DE BOLLE for the accessibility to the BSL-3 platform. We warmly thank Profs.

5   Jean-Pierre BRION, Karelle LEROY, Marielle BOONEN for providing neuroblastoma

6   and glioblastoma cell lines. We also thank Valérie DE GLAS and Catherine DEMAZY

7   for technical assistance. This research was made possible thanks to the access to the

8   microscope facility of the "Plateforme Technologique Morphologie – Imagerie"

9   (Université de Namur). This research did not receive any specific grant from funding

10   agencies in the public, commercial, or not-for-profit sectors.

11

12   **Author contribution**

13   Data curation, Formal analysis, Methodology: V.B., K.W., N.A., K.D, R.L., N.N.

14   Conceptualization, Writing – Original Draft Preparation: N.G., C.N.

15   Writing – Review & Editing: J.G., N.G.

16

17   **Conflicts of Interest**

18   The authors declare no conflict of interest.

19

20   **Submission declaration**

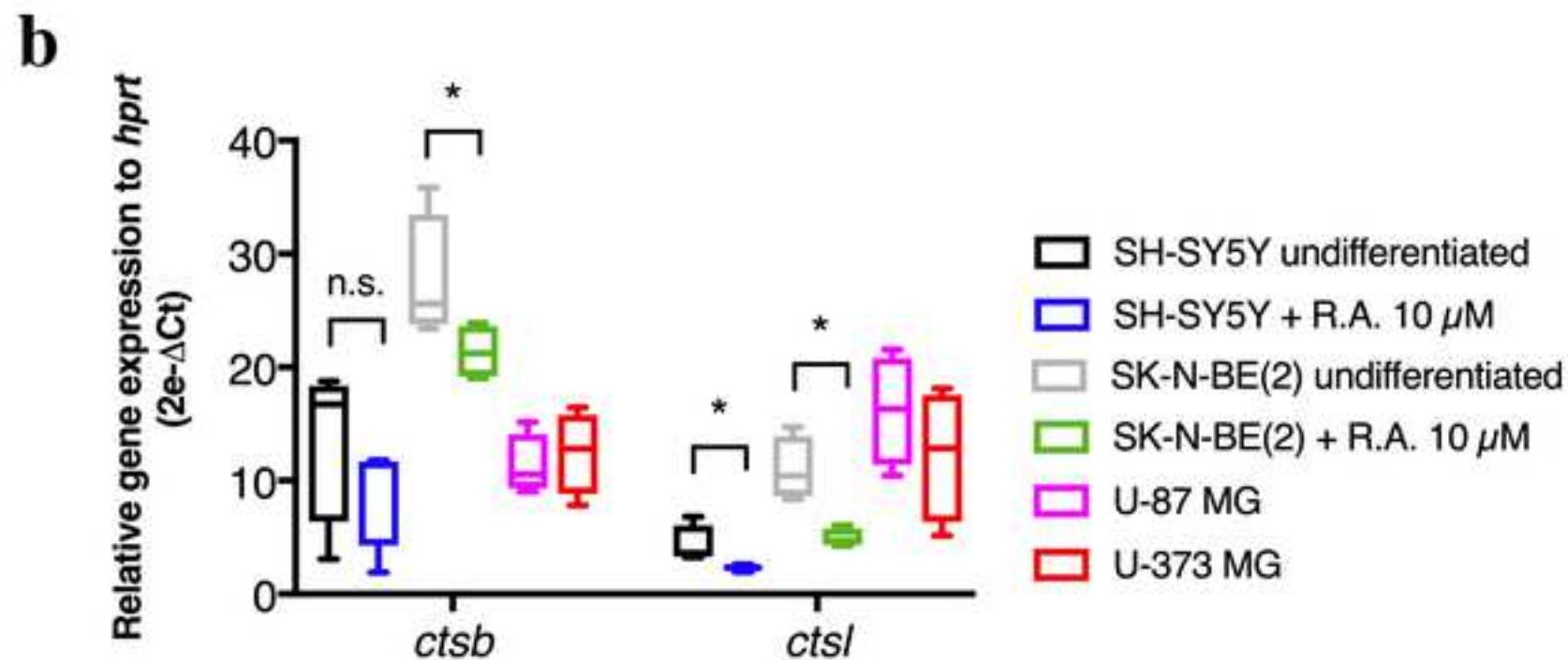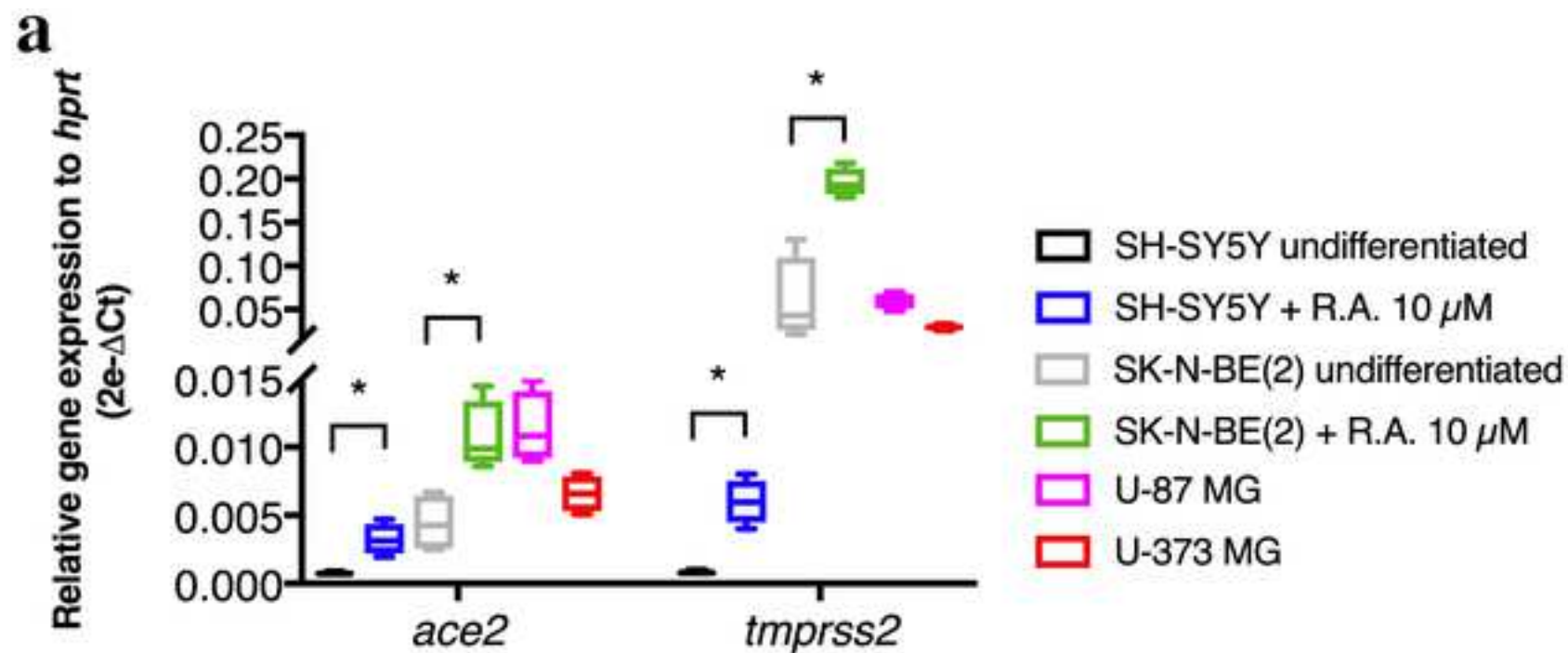21   This manuscript has not been published or is being reviewed elsewhere.
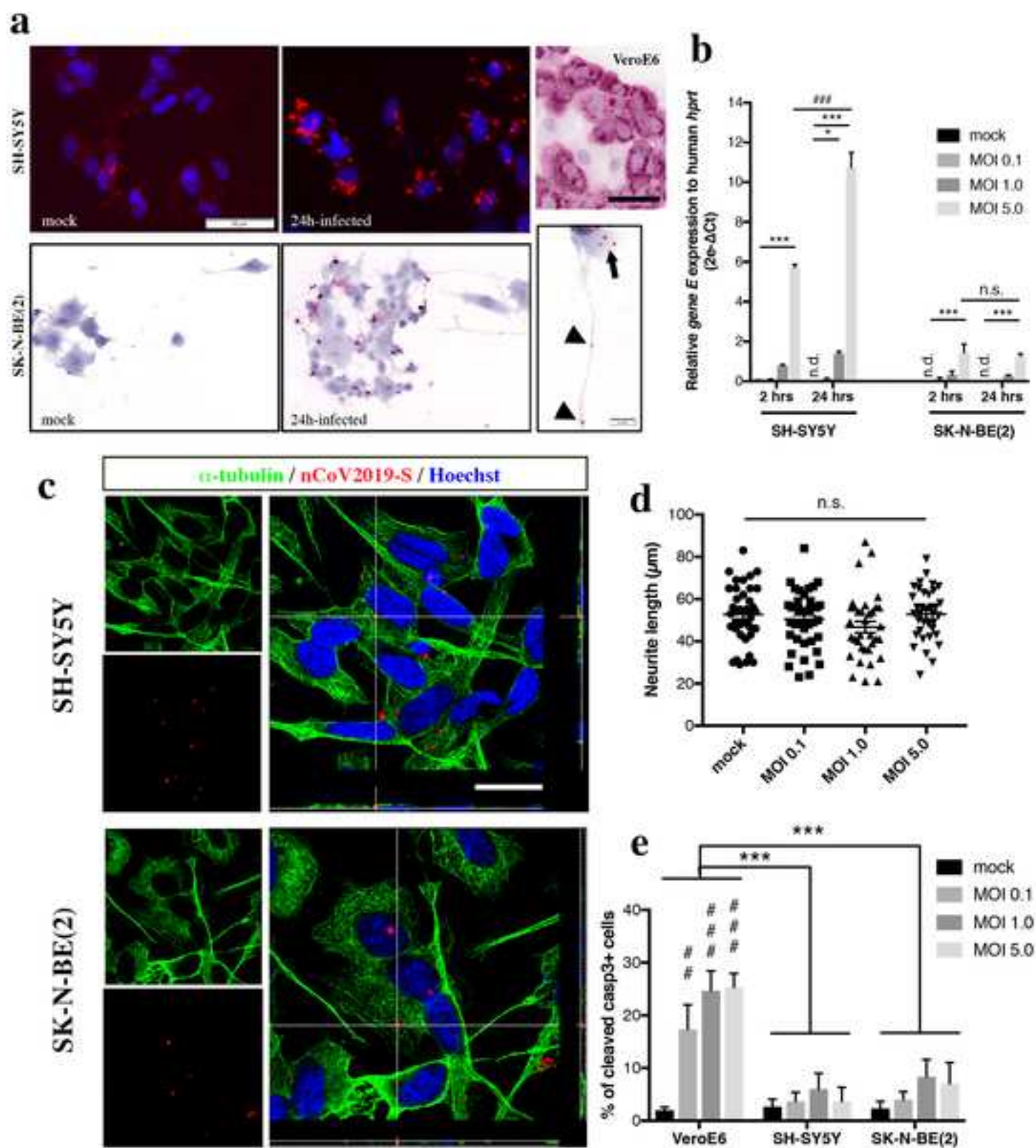
22

1 **References**

2 Asadi-Pooya, A.A., Simani, L., 2020. Central nervous system manifestations of COVID-19: A
3 systematic review. J Neurol Sci. 413**,** 116832.
4 Bulfamante, G., Chiumello, D., Canevini, M.P., Priori, A., Mazzanti, M., Centanni, S., Felisati,
5 G., 2020. First ultrastructural autoptic findings of SARS -Cov-2 in olfactory pathways and
6 brainstem. Minerva Anestesiol. 86**,** 678-679.
7 Bullen, C.K., Hogberg, H.T., Bahadirli-Talbott, A., Bishai, W.R., Hartung, T., Keuthan, C.,
8 Looney, M.M., Pekosz, A., Romero, J.C., Sillé, F.C.M., Um, P., Smirnova, L., 2020.
9 Infectability of human BrainSphere neurons suggests neurotropism of SARS-CoV-2. Altex. 37**,**
10 665-671.
11 Cantuti-Castelvetri, L., Ojha, R., Pedro, L.D., Djannatian, M., Franz, J., Kuivanen, S., van der
12 Meer, F., Kallio, K., Kaya, T., Anastasina, M., Smura, T., Levanov, L., Szirovicza, L., Tobi,
13 A., Kallio-Kokko, H., Österlund, P., Joensuu, M., Meunier, F.A., Butcher, S.J., Winkler, M.S.,
14 Mollenhauer, B., Helenius, A., Gokce, O., Teesalu, T., Hepojoki, J., Vapalahti, O., Stadelmann,
15 C., Balistreri, G., Simons, M., 2020. Neuropilin-1 facilitates SARS-CoV-2 cell entry and
16 infectivity. Science. 370**,** 856-860.
17 Chen, N., Zhou, M., Dong, X., Qu, J., Gong, F., Han, Y., Qiu, Y., Wang, J., Liu, Y., Wei, Y.,
18 Xia, J., Yu, T., Zhang, X., Zhang, L., 2020. Epidemiological and clinical characteristics of 99
19 cases of 2019 novel coronavirus pneumonia in Wuhan, China: a descriptive study. Lancet. 395**,**
20 507-513.
21 Chu, H., Chan, J.F., Yuen, T.T., Shuai, H., Yuan, S., Wang, Y., Hu, B., Yip, C.C., Tsang, J.O.,
22 Huang, X., Chai, Y., Yang, D., Hou, Y., Chik, K.K., Zhang, X., Fung, A.Y., Tsoi, H.W., Cai,
23 J.P., Chan, W.M., Ip, J.D., Chu, A.W., Zhou, J., Lung, D.C., Kok, K.H., To, K.K., Tsang, O.T.,
24 Chan, K.H., Yuen, K.Y., 2020. Comparative tropism, replication kinetics, and cell damage
25 profiling of SARS-CoV-2 and SARS-CoV with implications for clinical manifestations,
26 transmissibility, and laboratory studies of COVID-19: an observational study. Lancet Microbe.
27 1**,** e14-e23.
28 Coolen, T., Lolli, V., Sadeghi, N., Rovai, A., Trotta, N., Taccone, F.S., Creteur, J., Henrard, S.,
29 Goffard, J.C., De Witte, O., Naeije, G., Goldman, S., De Tiege, X., 2020. Early postmortem
30 brain MRI findings in COVID-19 non-survivors. Neurology.
31 Coupeau, D., Burton, N., Lejeune, N., Loret, S., Petit, A., Pejakovic, S., Poulain, F., Bonil, L.,
32 Trozzi, G., Wiggers, L., Willemart, K., André, E., Laenen, L., Cuypers, L., Van Ranst, M.,
33 Bogaerts, P., Muylkens, B., Gillet, N.A., 2020. SARS-CoV-2 Detection for Diagnosis Purposes
34 in the Setting of a Molecular Biology Research Lab. Methods Protoc. 3.
35 Gu, J., Gong, E., Zhang, B., Zheng, J., Gao, Z., Zhong, Y., Zou, W., Zhan, J., Wang, S., Xie,
36 Z., Zhuang, H., Wu, B., Zhong, H., Shao, H., Fang, W., Gao, D., Pei, F., Li, X., He, Z., Xu, D.,
37 Shi, X., Anderson, V.M., Leong, A.S., 2005. Multiple organ infection and the pathogenesis of
38 SARS. J Exp Med. 202**,** 415-24.
39 Gupta, A., Madhavan, M.V., Sehgal, K., Nair, N., Mahajan, S., Sehrawat, T.S., Bikdeli, B.,
40 Ahluwalia, N., Ausiello, J.C., Wan, E.Y., Freedberg, D.E., Kirtane, A.J., Parikh, S.A., Maurer,
41 M.S., Nordvig, A.S., Accili, D., Bathon, J.M., Mohan, S., Bauer, K.A., Leon, M.B., Krumholz,
42 H.M., Uriel, N., Mehra, M.R., Elkind, M.S.V., Stone, G.W., Schwartz, A., Ho, D.D., Bilezikian,
43 J.P., Landry, D.W., 2020. Extrapulmonary manifestations of COVID-19. Nat Med. 26**,** 1017-
44 1032.
45 Helms, J., Kremer, S., Merdji, H., Clere-Jehl, R., Schenck, M., Kummerlen, C., Collange, O.,
46 Boulay, C., Fafi-Kremer, S., Ohana, M., Anheim, M., Meziani, F., 2020. Neurologic Features
47 in Severe SARS-CoV-2 Infection. N Engl J Med. 382**,** 2268-2270.
48 Hoffmann, M., Kleine-Weber, H., Schroeder, S., Krüger, N., Herrler, T., Erichsen, S.,
49 Schiergens, T.S., Herrler, G., Wu, N.H., Nitsche, A., Müller, M.A., Drosten, C., Pöhlmann, S.,

1   2020. SARS-CoV-2 Cell Entry Depends on ACE2 and TMPRSS2 and Is Blocked by a
2   Clinically Proven Protease Inhibitor. Cell. 181**,** 271-280.e8.
3   Kanberg, N., Ashton, N.J., Andersson, L.M., Yilmaz, A., Lindh, M., Nilsson, S., Price, R.W.,
4   Blennow, K., Zetterberg, H., Gisslén, M., 2020. Neurochemical evidence of astrocytic and
5   neuronal injury commonly found in COVID-19. Neurology. 95**,** e1754-e1759.
6   Kilinc, D., van de Pasch, S., Doets, A.Y., Jacobs, B.C., van Vliet, J., Garssen, M.P.J., 2020.
7   Guillain-Barré syndrome after SARS-CoV-2 infection. Eur J Neurol.
8   Kumari, P., Rothan, H.A., Natekar, J.P., Stone, S., Pathak, H., Strate, P.G., Arora, K., Brinton,
9   M.A., Kumar, M., 2021. Neuroinvasion and Encephalitis Following Intranasal Inoculation of
10   SARS-CoV-2 in K18-hACE2 Mice. Viruses. 13.
11   Lu, R., Zhao, X., Li, J., Niu, P., Yang, B., Wu, H., Wang, W., Song, H., Huang, B., Zhu, N.,
12   Bi, Y., Ma, X., Zhan, F., Wang, L., Hu, T., Zhou, H., Hu, Z., Zhou, W., Zhao, L., Chen, J.,
13   Meng, Y., Wang, J., Lin, Y., Yuan, J., Xie, Z., Ma, J., Liu, W.J., Wang, D., Xu, W., Holmes,
14   E.C., Gao, G.F., Wu, G., Chen, W., Shi, W., Tan, W., 2020. Genomic characterisation and
15   epidemiology of 2019 novel coronavirus: implications for virus origins and receptor binding.
16   Lancet. 395**,** 565-574.
17   Mahmoud, S., Gharagozloo, M., Simard, C., Gris, D., 2019. Astrocytes Maintain Glutamate
18   Homeostasis in the CNS by Controlling the Balance between Glutamate Uptake and Release.
19   Cells. 8.
20   Mao, L., Jin, H., Wang, M., Hu, Y., Chen, S., He, Q., Chang, J., Hong, C., Zhou, Y., Wang, D.,
21   Miao, X., Li, Y., Hu, B., 2020a. Neurologic Manifestations of Hospitalized Patients With
22   Coronavirus Disease 2019 in Wuhan, China. JAMA Neurol. 77**,** 683-690.
23   Mao, L., Wang, M., Chen, S., He, Q., Chang, J., Hong, C., Zhou, Y., Wang, D., Li, Y., Jin, H.,
24   Hu, B., 2020b. Neurological Manifestations of Hospitalized Patients with COVID-19 in
25   Wuhan, China: a retrospective case series study. medRxiv. 2020.02.22.20026500.
26   Meinhardt, J., Radke, J., Dittmayer, C., Franz, J., Thomas, C., Mothes, R., Laue, M., Schneider,
27   J., Brünink, S., Greuel, S., Lehmann, M., Hassan, O., Aschman, T., Schumann, E., Chua, R.L.,
28   Conrad, C., Eils, R., Stenzel, W., Windgassen, M., Rößler, L., Goebel, H.H., Gelderblom, H.R.,
29   Martin, H., Nitsche, A., Schulz-Schaeffer, W.J., Hakroush, S., Winkler, M.S., Tampe, B.,
30   Scheibe, F., Körtvélyessy, P., Reinhold, D., Siegmund, B., Kühl, A.A., Elezkurtaj, S., Horst,
31   D., Oesterhelweg, L., Tsokos, M., Ingold-Heppner, B., Stadelmann, C., Drosten, C., Corman,
32   V.M., Radbruch, H., Heppner, F.L., 2020. Olfactory transmucosal SARS-CoV-2 invasion as a
33   port of central nervous system entry in individuals with COVID-19. Nat Neurosci.
34   Moriguchi, T., Harii, N., Goto, J., Harada, D., Sugawara, H., Takamino, J., Ueno, M., Sakata,
35   H., Kondo, K., Myose, N., Nakao, A., Takeda, M., Haro, H., Inoue, O., Suzuki-Inoue, K.,
36   Kubokawa, K., Ogihara, S., Sasaki, T., Kinouchi, H., Kojin, H., Ito, M., Onishi, H., Shimizu,
37   T., Sasaki, Y., Enomoto, N., Ishihara, H., Furuya, S., Yamamoto, T., Shimada, S., 2020. A first
38   case of meningitis/encephalitis associated with SARS-Coronavirus-2. Int J Infect Dis. 94**,** 55-
39   58.
40   Netland, J., Meyerholz, D.K., Moore, S., Cassell, M., Perlman, S., 2008. Severe acute
41   respiratory syndrome coronavirus infection causes neuronal death in the absence of encephalitis
42   in mice transgenic for human ACE2. J Virol. 82**,** 7264-75.
43   Ortiz, M.E., Thurman, A., Pezzulo, A.A., Leidinger, M.R., Klesney-Tait, J.A., Karp, P.H., Tan,
44   P., Wohlford-Lenane, C., McCray, P.B., Jr., Meyerholz, D.K., 2020. Heterogeneous expression
45   of the SARS-Coronavirus-2 receptor ACE2 in the human respiratory tract. EBioMedicine. 60**,**
46   102976.
47   Paniz-Mondolfi, A., Bryce, C., Grimes, Z., Gordon, R.E., Reidy, J., Lednicky, J., Sordillo,
48   E.M., Fowkes, M., 2020. Central nervous system involvement by severe acute respiratory
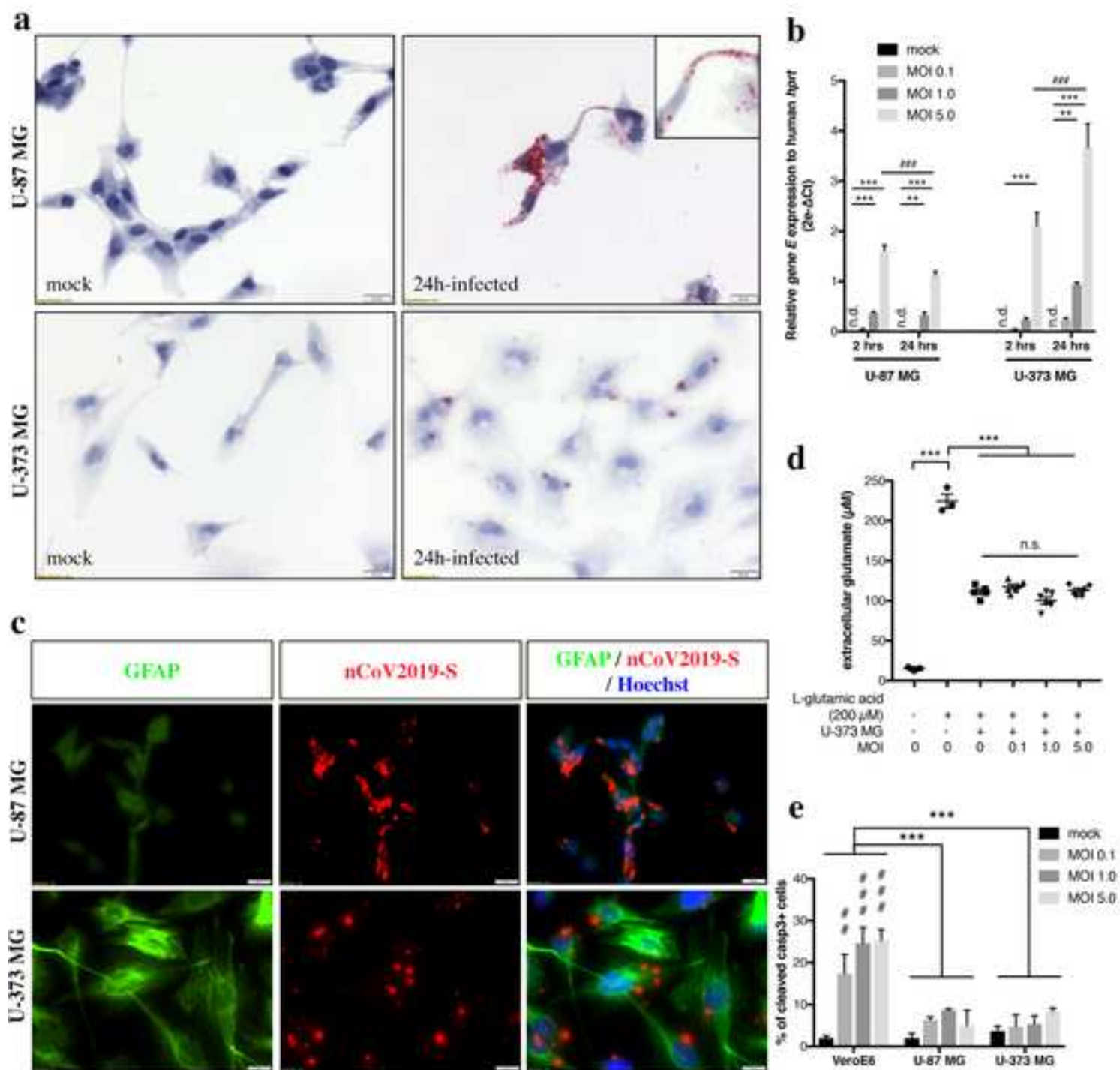49   syndrome coronavirus-2 (SARS-CoV-2). J Med Virol. 92**,** 699-702.

1   Paterson, R.W., Brown, R.L., Benjamin, L., Nortley, R., Wiethoff, S., Bharucha, T., Jayaseelan, D.L., Kumar, G., Raftopoulos, R.E., Zambreanu, L., Vivekanandam, V., Khoo, A., Geraldes, R., Chinthapalli, K., Boyd, E., Tuzlali, H., Price, G., Christofi, G., Morrow, J., McNamara, P., McLoughlin, B., Lim, S.T., Mehta, P.R., Levee, V., Keddie, S., Yong, W., Trip, S.A., Foulkes, A.J.M., Hotton, G., Miller, T.D., Everitt, A.D., Carswell, C., Davies, N.W.S., Yoong, M., Attwell, D., Sreedharan, J., Silber, E., Schott, J.M., Chandratheva, A., Perry, R.J., Simister, R., Checkley, A., Longley, N., Farmer, S.F., Carletti, F., Houlihan, C., Thom, M., Lunn, M.P., Spillane, J., Howard, R., Vincent, A., Werring, D.J., Hoskote, C., Jäger, H.R., Manji, H., Zandi, M.S., 2020. The emerging spectrum of COVID-19 neurology: clinical, radiological and laboratory findings. Brain. 143**,** 3104-3120.

2   Pemberton, K., Mersman, B., Xu, F., 2018. Using ImageJ to Assess Neurite Outgrowth in Mammalian Cell Cultures: Research Data Quantification Exercises in Undergraduate Neuroscience Lab. J Undergrad Neurosci Educ. 16**,** A186-a194.

3   Poyiadji, N., Shahin, G., Noujaim, D., Stone, M., Patel, S., Griffith, B., 2020. COVID-19-associated Acute Hemorrhagic Necrotizing Encephalopathy: CT and MRI Features. Radiology. 201187.

4   Puelles, V.G., Lütgehetmann, M., Lindenmeyer, M.T., Sperhake, J.P., Wong, M.N., Allweiss, L., Chilla, S., Heinemann, A., Wanner, N., Liu, S., Braun, F., Lu, S., Pfefferle, S., Schröder, A.S., Edler, C., Gross, O., Glatzel, M., Wichmann, D., Wiech, T., Kluge, S., Pueschel, K., Aepfelbacher, M., Huber, T.B., 2020. Multiorgan and Renal Tropism of SARS-CoV-2. N Engl J Med. 383**,** 590-592.

5   Radzikowska, U., Ding, M., Tan, G., Zhakparov, D., Peng, Y., Wawrzyniak, P., Wang, M., Li, S., Morita, H., Altunbulakli, C., Reiger, M., Neumann, A.U., Lunjani, N., Traidl-Hoffmann, C., Nadeau, K.C., O'Mahony, L., Akdis, C., Sokolowska, M., 2020. Distribution of ACE2, CD147, CD26, and other SARS-CoV-2 associated molecules in tissues and immune cells in health and in asthma, COPD, obesity, hypertension, and COVID-19 risk factors. Allergy. 75**,** 2829-2845.

6   Ramani, A., Müller, L., Ostermann, P.N., Gabriel, E., Abida-Islam, P., Müller-Schiffmann, A., Mariappan, A., Goureau, O., Gruell, H., Walker, A., Andrée, M., Hauka, S., Houwaart, T., Dilthey, A., Wohlgemuth, K., Omran, H., Klein, F., Wieczorek, D., Adams, O., Timm, J., Korth, C., Schaal, H., Gopalakrishnan, J., 2020. SARS-CoV-2 targets neurons of 3D human brain organoids. Embo j. 39, e106230.

7   Song, E., Zhang, C., Israelow, B., Lu-Culligan, A., Prado, A.V., Skriabine, S., Lu, P., Weizman, O.E., Liu, F., Dai, Y., Szigeti-Buck, K., Yasumoto, Y., Wang, G., Castaldi, C., Heltke, J., Ng, E., Wheeler, J., Alfajaro, M.M., Levavasseur, E., Fontes, B., Ravindra, N.G., Van Dijk, D., Mane, S., Gunel, M., Ring, A., Kazmi, S.A.J., Zhang, K., Wilen, C.B., Horvath, T.L., Plu, I., Haik, S., Thomas, J.L., Louvi, A., Farhadian, S.F., Huttner, A., Seilhean, D., Renier, N., Bilguvar, K., Iwasaki, A., 2021. Neuroinvasion of SARS-CoV-2 in human and mouse brain. J Exp Med. 218.

8   Uversky, V.N., Elrashdy, F., Aljadawi, A., Ali, S.M., Khan, R.H., Redwan, E.M., 2020. Severe acute respiratory syndrome coronavirus 2 infection reaches the human nervous system: How? J Neurosci Res.

9   Yang, L., Han, Y., Nilsson-Payant, B.E., Gupta, V., Wang, P., Duan, X., Tang, X., Zhu, J., Zhao, Z., Jaffré, F., Zhang, T., Kim, T.W., Harschnitz, O., Redmond, D., Houghton, S., Liu, C., Naji, A., Ciceri, G., Guttikonda, S., Bram, Y., Nguyen, D.T., Cioffi, M., Chandar, V., Hoagland, D.A., Huang, Y., Xiang, J., Wang, H., Lyden, D., Borczuk, A., Chen, H.J., Studer, L., Pan, F.C., Ho, D.D., tenOever, B.R., Evans, T., Schwartz, R.E., Chen, S., 2020. A Human Pluripotent Stem Cell-based Platform to Study SARS-CoV-2 Tropism and Model Virus Infection in Human Cells and Organoids. Cell Stem Cell. 27**,** 125-136.e7.

10   Ye, Z.C., Sontheimer, H., 1999. Glioma cells release excitotoxic concentrations of glutamate. Cancer Res. 59**,** 4383-91.

Zanin, L., Saraceno, G., Panciani, P.P., Renisi, G., Signorini, L., Migliorati, K., Fontanella, M.M., 2020. SARS-CoV-2 can induce brain and spine demyelinating lesions. Acta Neurochir (Wien). 162**,** 1491-1494.

Zhang, B.Z., Chu, H., Han, S., Shuai, H., Deng, J., Hu, Y.F., Gong, H.R., Lee, A.C., Zou, Z., Yau, T., Wu, W., Hung, I.F., Chan, J.F., Yuen, K.Y., Huang, J.D., 2020. SARS-CoV-2 infects human neural progenitor cells and brain organoids. Cell Res. 30**,** 928-931.

Zhao, K., Huang, J., Dai, D., Feng, Y., Liu, L., Nie, S., 2020. Acute myelitis after SARS-CoV-2 infection: a case report. medRxiv. 2020.03.16.20035105.

Figure1

Click here to access/download;Figure;Figure1.tif ⬇

Figure2   Click here to access/download;Figure;Figure2_new.tif ⬇

Figure3

Click here to access/download
Electronic Supplementary Material (online publication only)
SupplFig1.tif

Bielarz *et al.*   SARS-CoV-2 infection of neural cell lines

1   **Author contribution**

2   Data curation, Formal analysis, Methodology: V.B., K.W., N.A., K.D, R.L., N.N.

3   Conceptualization, Writing – Original Draft Preparation: N.G., C.N.

4   Writing – Review & Editing: J.G., N.G.

5